JGR Biogeosciences

RESEARCH ARTICLE
10.1029/2022JG006798

The Role of Zooplankton Grazing and Nutrient Recycling for Global Ocean Biogeochemistry and Phytoplankton Phenology

Onur Karakuş[1], Christoph Völker[1], Morten Iversen[1,2], Wilhelm Hagen[2,3], and Judith Hauck[1]

[1]Alfred-Wegener-Institut Helmholtz-Zentrum für Polar- und Meeresforschung, Bremerhaven, Germany, [2]MARUM and University of Bremen, Bremen, Germany, [3]University of Bremen, BreMarE, Marine Zoology, Bremen, Germany

Abstract Zooplankton plays a notable role in ocean biogeochemical cycles. However, it is often simulated as one generic group and top closure term in ocean biogeochemical models. This study presents the description of three zooplankton functional types (zPFTs, micro-, meso- and macrozooplankton) in the ocean biogeochemical model FESOM-REcoM. In the presented model, microzooplankton is a fast-growing herbivore group, mesozooplankton is another major consumer of phytoplankton, and macrozooplankton is a slow-growing group with a low temperature optimum. Meso- and macrozooplankton produce fast-sinking fecal pellets. With three zPFTs, the annual mean zooplankton biomass increases threefold to 210 Tg C. The new food web structure leads to a 25% increase in net primary production and a 10% decrease in export production globally. Consequently, the export ratio decreases from 17% to 12% in the model. The description of three zPFTs reduces model mismatches with observed dissolved inorganic nitrogen and chlorophyll concentrations in the South Pacific and the Arctic Ocean, respectively. Representation of three zPFTs also strongly affects phytoplankton phenology: Fast nutrient recycling by zooplankton sustains higher chlorophyll concentrations in summer and autumn. Additional zooplankton grazing delays the start of the phytoplankton bloom by 3 weeks and controls the magnitude of the bloom peak in the Southern Ocean. As a result, the system switches from a light-controlled Sverdrup system to a dilution-controlled Behrenfeld system. Overall, the results suggest that representation of multiple zPFTs is important to capture underlying processes that may shape the response of ecosystems and ecosystem services to on-going and future environmental change in model projections.

Plain Language Summary Zooplankton plays an important role in the ocean food web and biogeochemical cycles. However, it is often represented in very simple forms in mathematical models that are, for example, used to investigate how marine primary productivity will react to climate change. To understand how these models would change when more complicated formulations for zooplankton are used, we present here a new version of the model with three (instead of only one) zooplankton groups. We find that this more complicated representation leads to higher zooplankton biomass, which is closer to observations, and this stimulates growth of phytoplankton since zooplankton also returns nutrients into the system. In addition, zooplankton grazing controls the seasonal cycle of phytoplankton, as we show for one example in the Southern Ocean.

Key Points:

- Nutrient recycling by zooplankton stimulates net primary production in the biogeochemical model REcoM-2
- Modeling zooplankton functional types (zPFTs) leads to a switch from a light-controlled Sverdrup system to a dilution-controlled Behrenfeld system
- Implementing multiple zPFTs improves the modeled zooplankton biomass and zooplankton-mediated biogeochemical fluxes

Supporting Information:

Supporting Information may be found in the online version of this article.

Correspondence to:

O. Karakuş,
onur.karakus@awi.de

Citation:

Karakuş, O., Völker, C., Iversen, M., Hagen, W., & Hauck, J. (2022). The role of zooplankton grazing and nutrient recycling for global ocean biogeochemistry and phytoplankton phenology. *Journal of Geophysical Research: Biogeosciences*, *127*, e2022JG006798. https://doi.org/10.1029/2022JG006798

Received 14 JAN 2022
Accepted 5 OCT 2022

1. Introduction

Marine zooplankton forms an important component of the ocean ecosystem. It serves as a link between primary producers and higher trophic levels (Steinberg & Landry, 2017). Although zooplankton consists of a large variety of taxa from unicellular flagellates to multicellular organisms like copepods, it can be classified into five different size classes; nano (2–20 µm, e.g., flagellates), micro (20–200 µm, e.g., ciliates), meso (0.2–20 mm, e.g., copepods), macro (2–20 cm, e.g., krill) and mega (0.2–2 m, e.g., jellyfish; Sieburth et al., 1978). These different size classes of zooplankton have distinct functions in the ecosystem. For example, microzooplankton consume almost 60% of the daily primary production as major grazers of phytoplankton (Calbet, 2008; Landry & Calbet, 2004), while mesozooplankton and macrozooplankton produce fast sinking particulate matter as fecal pellets, which can contribute the highest share to carbon flux (Turner, 2002, 2015). These groups also prefer different prey. While meso- and macrozooplankton prefer larger prey items such as diatoms and smaller zooplankton, microzooplankton prefer smaller organisms such as smaller phytoplankton (Calbet & Landry, 1999; Hansen et al., 1994; Schmidt et al., 2014). Additionally, meso- and macrozooplankton release nutrients via sloppy feeding and excretion (Cavan et al., 2019; Saba et al., 2009). Zooplankton can therefore stimulate phytoplankton growth (Coello-Camba

et al., 2017) and meso- and microzooplankton nutrient regeneration can support 11%–25% of primary and bacterial production (Hernández-León et al., 2008; Verity, 1985).

The first ocean ecosystem models represented zooplankton with just one model state variable (Frost, 1987) and this is still common in the majority of ocean biogeochemical models used for projections of the global carbon cycle and marine primary productivity (Séférian et al., 2020). A minority of models uses multiple zooplankton functional types (zPFTs), such as COBALTv2 (small, medium and large zooplankton; Stock et al., 2020), PLANKTOM-11 (proto-, meso-, macrozooplankton and jellyfish; Wright et al., 2020), PISCESv2 (micro- and mesozooplankton; Aumont et al., 2015), MEDUSA (micro- and mesozooplankton; Yool et al., 2013). Yet the effect of representing multiple zPFTs in biogeochemical models has hardly been studied and documented, and the question remains whether this additional complexity adds sufficient improvement to a model state to justify its computational cost and the added uncertainty due to more parameters (Anderson, 2005). Pioneering studies, such as Le Quéré et al. (2016) showed the pivotal role of a slow-growing macrozooplankton functional type to obtain a realistic north-south chlorophyll ratio in a biogeochemical model. Also, the implementation of micro- and mesozooplankton functional types improved the formation of sinking particles, grazing and nutrient recycling by zooplankton in the same model (Buitenhuis et al., 2006, 2010). Recently, Wright et al. (2020) showed that predation pressure of jellyfish changed the macrozooplankton biomass and distribution due to competition in a three-dimensional ocean biogeochemical model.

While model development on representing zooplankton types and processes is underway, the level of complexity covered by different models spans a wide range. The number of zPFTs and their traits (parameters, processes) still represent major differences among models and cause for uncertainty in model results (Laufkötter et al., 2016). For example, differences in zooplankton feeding preferences, mortality, and ingestion rates can result in three times higher or lower zooplankton and phytoplankton biomass in modeled plankton food webs (Mitra et al., 2014). Also, prey-ratio based predation schemes such as a type III or active switching formulations improve the phytoplankton succession and increase phytoplankton diversity in a global model (Prowe et al., 2012). Similarly, the choice of different grazing formulations (Michaelis-Menten, Blackman, or Ivlev) can cause three times higher surface diatom concentrations in a global biogeochemical model (Anderson et al., 2013). Furthermore, diel vertical migration (grazing refuge) to escape predation for zooplankton can impact the model results. Diel vertical migration is generally not included, since biogeochemical models are limited in the complexity of represented processes, but first parameterizations were recently suggested. For example, Archibald et al. (2019) showed that parametrizing zooplankton diel vertical migration increases the modeled global export flux by 14% in the global ocean. Also, Chenillat et al. (2021) indicated that different grazing refuge formulations cause large changes in plankton diversity, structure, and ecosystem functioning in a regional modeling study.

One under-exploited aspect to assess the model performance with respect to zooplankton processes is the phytoplankton bloom phenology. To first order, models can reproduce major bloom properties and their timing (phenology) since growth rates of phytoplankton depend on abiotic factors (Behrenfeld & Boss, 2018; Sverdrup, 1953). However, top-down mechanisms can also control phytoplankton bloom initiation due to ecosystem imbalances (Behrenfeld et al., 2013) and bloom termination due to overgrazing (Banse, 1992, 2002). Hence, phytoplankton phenology is directly connected with predator-prey relationships and the parametrization of several grazers in the system. Timing of grazing losses and predator-prey decoupling is vital to capture the phytoplankton bloom timing (Banse, 2013; Behrenfeld et al., 2013; Kiørboe, 1997). Pioneering studies by Frost (1991, 1993), and Banse (1994) showed that grazers often control phytoplankton stock and production in the open ocean. Recently, Hashioka et al. (2013) and Nissen and Vogt (2021) have discussed the early phytoplankton bloom peak compared to satellite products in biogeochemical models, which could be caused by too weak zooplankton grazing in the Southern Ocean. Therefore, a better understanding of ecosystem functioning and phenology structures requires complex and well-defined grazing processes in the models. Phytoplankton phenology contains more information than only the mean state and can be used to evaluate how well a model represents the response of phytoplankton growth and loss (e.g., grazing, respiration) rates to processes such as deepening and shoaling of the mixed layer depth (MLD), changes in light availability, and nutrient variations over the year.

Here, we present a new version of REcoM-2 with three zPFTs (herbivorous microzooplankton, omnivorous mesozooplankton, and omnivorous macrozooplankton) and compare this to a previous version with one herbivorous zooplankton group. To analyze the impact of zPFTs, we discuss the changes in the mean states (phytoplankton and zooplankton biomass, productivity, nutrient fields), and attribute these differences to nutrient excretion

and grazing by zooplankton. We then exemplarily analyze the effect of zooplankton representation on the phytoplankton bloom phenology in the Southern Ocean within the global ocean biogeochemical model.

2. Methods

2.1. Ocean Biogeochemical Model

We use a three-dimensional ocean biogeochemical model, namely the Regulated Ecosystem Model (REcoM-2; Hauck et al., 2013; Schourup-Kristensen et al., 2014) coupled to the Finite Element Sea-Ice Ocean Model FESOM-1.4 (Wang et al., 2014). Originally, REcoM-2 has two phytoplankton classes (small phytoplankton and diatoms) and one zooplankton group. It represents the carbonate system and resolves the cycling of the nutrients nitrate, silicic acid and iron. Phytoplankton stoichiometry varies with environmental conditions (variable N:C:Chl:Si for diatoms and N:C:Chl for small phytoplankton, Geider et al., 1998) and the sinking of particles is simulated explicitly. For representing the global ocean, we use the CORE-II mesh, roughly comparable to a global $1 \times 1^{\circ}$ resolution. It has a higher resolution (20–70 km) in dynamical areas and coarser resolution in less dynamic areas (100–120 km), for example, subtropical areas (Sidorenko et al., 2011).

2.2. Zooplankton and Sinking Particles in the Model

In addition to the original version of REcoM-2 (with one zooplankton group), we already implemented a polar macrozooplankton group (parametrized as Antarctic Krill) and a fast-sinking detritus class (Karakuş et al., 2021). In this study, we go one step further and separate the herbivore group into the microzooplankton and mesozooplankton groups. The general structure of the rate of change in biomass of zPFTs $\left(\frac{dZ}{dt}\right)$ can be described by the following text equation:

$$\frac{dZ}{dt} = Ingestion - excretion - egestion - respiration - mortality \quad (1)$$

Where the ingestion represents the biomass source to zooplankton (Z) which is grazing. The processes respiration, excretion, egestion and mortality are the sink terms for the zooplankton biomass. The complete set of zooplankton equations and parameter values are provided in the supplementary text. Here, we describe the main differences of zooplankton groups, grazing structure, and sinking particles in the two model versions.

In our zPFTs set-up, microzooplankton (<200 μm) is parameterized as a fast-growing herbivore group which is closely coupled to the growth of phytoplankton groups. They are the main grazers of phytoplankton in tropical and subtropical regions (60% of daily primary production) and their grazing usually exceeds that of mesozooplankton (Calbet, 2008; Landry & Calbet, 2004). This is represented by a high grazing rate of 0.42 (d^{-1}) at 0°C with a Q_{10} value of 1.48 taken from a data compilation by Le Quéré et al. (2016). The assimilation efficiency is set to 0.8 which is higher than for mesozooplankton and macrozooplankton (Le Quéré et al., 2016). The unassimilated part represents mini pellet production (Gowing & Silver, 1985) and all the sinking particles from this group go to the slow-sinking detritus class (Table 1). Microzooplankton has a feeding preference on small phytoplankton rather than on diatoms (Figure 1, Micro, Froneman & Perissinotto, 1996; Le Quéré et al., 2005). The respiration rate of microzooplankton is temperature-dependent using the Q_{10} value of 2.36 and a rate of 0.01 d^{-1} at 0°C is taken from Le Quéré et al. (2016). The production of dissolved organic material (DOM) by nitrogen and carbon excretion is assigned daily rate constants of 0.05 d^{-1} which is the same as for phytoplankton C and N excretion rates. The microzooplankton group is parametrized as prey for the mesozooplankton and macrozooplankton groups (Calbet, 2008).

The mesozooplankton group is another major consumer of phytoplankton (10% of daily primary production) in the global ocean (Calbet, 2008). Also, it produces large fast-sinking fecal pellets (Turner, 2002). We take these two main roles into account for the parametrization of this functional group. Mesozooplankton grazing rate is slower than that of microzooplankton and it is set to 0.31 d^{-1} at 0°C with a Q_{10} value of 1.27 (Le Quéré et al., 2016). Mesozooplankton produces large sinking particles (fecal pellets) and prefers feeding on large phytoplankton (diatoms in REcoM) and microzooplankton rather than on small phytoplankton (Calbet & Landry, 1999; Le Quéré et al., 2005; Mullin, 1963). It also grazes on both simulated detritus groups. Different

Table 1
Specifics of Zooplankton Functional Types (zPFTs): Grazing on Various Food Sources, Routing of Sinking Particles Into Slow and Fast Sinking Detritus Classes in the Model, Grazing Rate and Temperature Dependency (Q_{10} Value)

	REcoM-2	REcoM-3ZOO		
	One Zooplankton group	Microzoo	Mesozoo	Macrozoo
Grazing on diatoms	X	X	X	X
Grazing on small phytoplankton	X	X	X	X
Grazing on microzooplankton	–	–	X	X
Grazing on mesozooplankton	–	–	–	X
Grazing on detritus	–	–	X	X
Slow-sinking sPOC	X	X	–	–
Fast-sinking sPOC	–	–	X	X
Grazing rate at 0°C (d^{-1})	1	0.46	0.31	0.1
Q_{10} value	1.80	1.48	1.27	See supplementary text

Note. All equations and parameter values as well as their references are listed in the supplementary material.

from microzooplankton, a part of the grazed material is lost and routed to detritus ("sloppy feeding"). Sloppy feeding is set to 20% of the grazing flux (Steinberg & Landry, 2017) initially and it increases with increasing food concentration as described in Roy et al. (1989) and Montagnes and Fenton (2012). The assimilation efficiency of ingested carbon and nitrogen is set to 68% and 75% for nitrogen and carbon respectively to mimic the higher C:N ratio in fecal pellets (Morales, 1987). All the sinking particles from mesozooplankton go to the fast-sinking detritus class (Table 1). The respiration rate of mesozooplankton is temperature-dependent using a Q_{10} value of 2.34 and a rate 0.028 d^{-1} at 0°C is taken from Le Quéré et al. (2016). We acknowledge that this is a simplification and mesozooplankton respiration rate could be described as a combination of basal and food-dependent components as for example, Kiørboe et al. (1985) and Thor (2003) describe copepod respiration to vary with food availability. The DOC and DON excretion rate constants are set higher than for microzooplankton with 0.1 d^{-1}, in line with an estimate based on Hernández-León et al. (2008) of 12% between 50°N and 50°S.

The macrozooplankton group is parametrized as krill (Karakuş et al., 2021) and mainly represents the polar macrozooplankton in the model with a maximum grazing rate at a temperature optimum of 0.5°C. Sloppy feeding was set to 20% for macrozooplankton and this group produces large fecal pellets with a high C:N ratio. The sinking particles from the macrozooplankton group were assigned to the fast-sinking detritus class (Table 1). Macrozooplankton grazes on phytoplankton, zooplankton, and both detritus groups and has a lower grazing

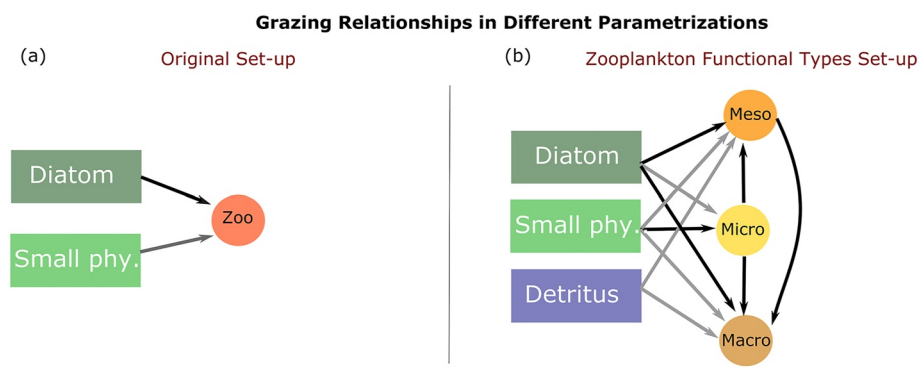

Figure 1. Grazing relations in the two model versions: (a) Original REcoM-2, (b) Zooplankton functional types set-up. The colors of the arrows indicate the initial relative preferences (parameter values can be found in the supplementary text), black shows the preferred food source for the zooplankton functional type. Multiple black lines indicate an equal grazing preference. Micro: microzooplankton feeds on diatoms, and small phytoplankton. Meso: mesozooplankton feeds on diatoms, small phytoplankton, detritus and microzooplankton. Macro: macrozooplankton feeds on diatoms, small phytoplankton, detritus, microzooplankton, and mesozooplankton.

preference for small phytoplankton than for diatoms and other zooplankton groups. DOC and DON excretion rate constants were set to 0.02 d^{-1} (Atkinson et al., 2002). Differently from the other zooplankton groups, the respiration rate of the macrozooplankton group is down-regulated during winter and at low food availability (Hofmann & Lascara, 2000).

2.3. Simulations

We conduct two simulations to analyze the impact of the representation of zooplankton in the model. One simulation is carried out with REcoM-2 (with one zooplankton group) and the other simulation with REcoM-3ZOO (with three zPFTs). The global model is forced with the JRA-55-do atmospheric forcing data set version 1.3.1 (Kobayashi et al., 2015) in 60 years long simulations. Repeated year forcing fields from the year 1961 of surface rainfall, and snowfall fluxes, as well as near-surface (2 m) air temperature, specific humidity, surface downwelling short- and long-wave radiation, eastward and northward wind components, and sea level pressure for the years 1958–2017, are used. Freshwater runoff and the surface salinity field for a weak surface salinity restoring (Sidorenko et al., 2011) are taken from the CORE-II climatology (Griffies et al., 2009). The nutrients dissolved silicic acid (DSi) and dissolved inorganic nitrogen (DIN) are initialized with World Ocean Atlas 2013 products (Garcia et al., 2013), and alkalinity and dissolved inorganic carbon from GLODAPv2 (Lauvset et al., 2016).

The global nutrients, chlorophyll concentrations, and zooplankton biomass are analyzed for the surface annual mean over the last 5 years of the model simulation by using monthly model output. Daily output from the last 5 years of the chlorophyll and phytoplankton biomass is used to assess the impact of zooplankton processes on phytoplankton phenology.

2.4. Bloom Phenology Evaluation and Skill Assessment

In this study, we use two different methods to assess the surface phytoplankton bloom phenology. The first method uses the surface phytoplankton carbon biomass (P_C, mmol C m^{-3}) and its accumulation rate (r, d^{-1}) as a metric (Llort et al., 2015) and the second one uses the surface chlorophyll concentration with a given threshold (Siegel et al., 2002).

In the first method, we decompose the bloom phenology into onset, climax, and apex as described in Llort et al. (2015). The net biomass accumulation rate (r, d^{-1}) was used to define these three events (Equation 2).

$$r = \frac{1}{P_C} \cdot \frac{dP_C}{dt} \tag{2}$$

The bloom onset is the day when total biomass (P_C, mmol C m^{-3}) starts to increase. On this day, biomass is at its minimum, the net accumulation rate (r, d^{-1}) equals zero and the temporal derivative (dr/dt) is greater than zero. On the climax day, the bloom accumulation rate is maximum and its time derivative equals zero. Finally, the bloom apex is defined as the day when total phytoplankton biomass (P_C, mmol C m^{-3}) reaches its maximum, the net accumulation rate (r, d^{-1}) is zero and its time derivative (dr/dt) is negative.

In the second method, we identify the bloom start, peak, and end days by using surface chlorophyll concentrations (Siegel et al., 2002). For comparison with satellite products, we disregard model output during times when no observations are available (May–August). The first day when chlorophyll concentration is higher than the threshold value is the bloom start day (BSD), the day when chlorophyll concentration reaches a maximum is bloom peak day and finally, the day when chlorophyll concentration is below the threshold is the bloom end day (BED). However, we should acknowledge that even though this method is used widely (Henson et al., 2009; Racault et al., 2012; Soppa et al., 2016), the result depends on the chosen threshold value (Racault et al., 2012). In this study, we use a threshold value of 5% above the median as in Soppa et al. (2016).

A Taylor diagram (Taylor, 2001) was used to assess the performance of the two model versions. We used the OC-CCI satellite surface chlorophyll concentration product (Sathyendranath et al., 2019), the remotely sensed net primary production (NPP) data sets VGPM (Behrenfeld & Falkowski, 1997), and CPBM (Westberry et al., 2008) as well as the World Ocean Atlas nutrient fields (Garcia et al., 2018) to assess the global surface macronutrient and chlorophyll concentration results of the model simulations (Figure 3). To assess the Southern Ocean bloom phenology, the surface chlorophyll satellite product (2003–2013) of Johnson et al. (2013) was used.

Table 2
Global Annual Total Values for Net Primary Production (NPP), Export Production (EP) at 100 m and Plankton Functional Types Biomass From Observations and Previous Studies, REcoM-2 and REcoM-3ZOO

	REcoM-2	REcoM-3ZOO	Data - Previous studies
Rates (Pg C yr^{-1})			
NPP	30.3	38	47.3 (Behrenfeld & Falkowski, 1997)*
			35-70 (Carr et al., 2006; Kulk et al., 2021)*
			51–65 (Buitenhuis et al., 2013)°
EP at 100 m	5.2	4.7	9–10 (Schlitzer, 2004; Lee, 2001)*
			5.8–13.0 (Dunne et al., 2007)*
			5 (Henson et al., 2011)+
			6 (Siegel et al., 2014)*
Integrated phytoplankton biomass over the upper 200 m (Tg C)			
Small-phy.	730	830	—
Diatom	380	330	13–750 (Leblanc et al., 2012)+
Integrated zooplankton biomass over the upper 200 m (Tg C)			
Microzoo.	—	160	100–370 (Buitenhuis et al., 2010)+
Mesozoo.	60	30	210–340 (Moriarty & O'Brien, 2013)+
Macrozoo.	—	20	10–640 (Moriarty et al., 2013)+
* Remote sensing,	+ Observations,	° Models	

Note. Model results are averaged over the last 5 years.

2.5. Analysis on Zooplankton Grazing and Nutrient Excretion

We focus on two main processes: the grazing loss of phytoplankton due to zooplankton grazing and the total nutrient recycling by all zooplankton groups. The total grazing loss of phytoplankton (Equation 3, $Phy_{grzloss}$, d^{-1}) is calculated by dividing the total zooplankton grazing rate ($\sum_i G_i$, i = each zooplankton, mmol C m^{-3} d^{-1}) through the total phytoplankton biomass concentration (P_C, mmol C m^{-3}). The total DON excretion by zooplankton (Equation 4, Zoo_{excr}, mmol N m^{-3} d^{-1}) is calculated as the sum of the product of total zooplankton biomass (Z_N, mmol N m^{-3}) times the excretion rate constants of each zooplankton group (ϵ_{Z_i}). Iron excretion is directly converted from DON excretion as the model assumes a constant N:Fe ratio of 0.033 (mmol/μmol).

$$Phy_{grzloss} = \frac{\sum_i G_i}{P_C} \tag{3}$$

$$Zoo_{excr} = \sum_i Z_{N_i} \cdot \epsilon_{Z_i} \tag{4}$$

3. Results

3.1. Global Ecosystem Properties in the REcoM-3ZOO Model

In REcoM-3ZOO, microzooplankton has the highest biomass integrated over the top 200 m (160 Tg C) among the zooplankton groups, followed by mesozooplankton (30 Tg C) and macrozooplankton (20 Tg C). We observe a significant increase and improvement in total zooplankton biomass representation in REcoM-3ZOO (Table 2). Modeled micro- and macrozooplankton biomasses are in the observational range (Buitenhuis et al., 2010; Moriarty & O'Brien, 2013), and microzooplankton is the major grazer in the model as reported from the observations (Steinberg & Landry, 2017). Although the global mean annual NPP grazed by microzooplankton is with 22% (NPP-weighted 26%, microzooplankton-biomass weighted 33%) lower than the 60% reported by Calbet and Landry (2004), the fraction of NPP grazed by microzooplankton varies spatially and reaches up to 70% in regions with high microzooplankton abundance (Figure S4 in Supporting Information S1). Given that there is currently

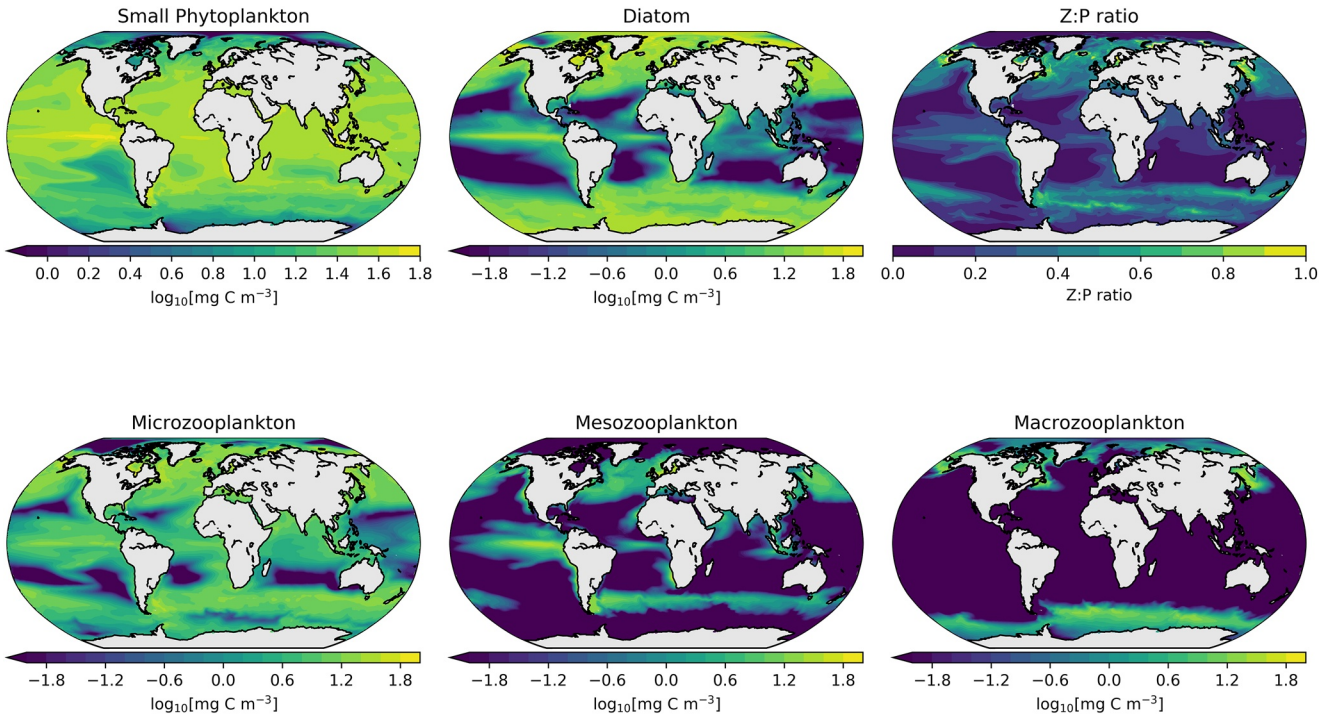

Figure 2. Annual mean surface carbon biomasses for plankton functional types in the REcoM-3ZOO model (log10 [mg C m^{-3}]) and the ratio of total zooplankton biomass to total phytoplankton biomass. Model results are averaged for the last 5 years of the simulations.

no instrumentation available to robustly quantify zooplankton grazing rates remotely or in situ (Menden-Deuer et al., 2021), we consider this a reasonable agreement. Modeled mesozooplankton biomass is relatively low in the model, but its contribution to grazing is well represented with about 10% of global NPP, which is similar to the estimate of 12% by Calbet (2001). Sensitivity simulations with higher mesozooplankton grazing rate or lower excretion rates led to a higher mesozooplankton biomass, but at the cost of strongly reducing microzooplankton biomass (not shown).

In both model versions, small phytoplankton group biomass is higher than the diatom biomass. While small phytoplankton amounts to 66% of total phytoplankton biomass in REcoM-2, this share increases to 72% in REcoM-3ZOO. The share of diatoms (28%) is still within the reported range of 20%–60% (Buitenhuis et al., 2013). The slight decrease (50 Tg C) in diatom biomass is a result of increased grazing pressure on diatoms after parametrizing meso- and macrozooplankton functional types. The ratio of total modeled zooplankton biomass to total phytoplankton biomass exhibits spatial variability and reaches 1:1 in coastal areas in the northern high latitudes (Figure 2). Because of the spatial variability, this ratio is also sensitive to the averaging procedure: The zooplankton biomass weighted mean Z:P ratio doubles from 0.26 in REcoM-2 to 0.51 in REcoM-3ZOO, and the phytoplankton biomass weighted mean Z:P ratio is 0.33 and thus five times higher in REcoM-3ZOO than in REcoM-2 (0.07).

Standing stocks of organic carbon and nutrients are transferred up the food chain to zooplankton in a model formulation with three zPFTs. Zooplankton partitions the carbon and nutrients initially bound by primary production between zooplankton growth, export and recycled production. This leads to a different model state with more recycling-fueled NPP at the expense of less export: The global annual mean NPP increases by 7.7 Pg C y^{-1} (25%) to 38 Pg C y^{-1} in the REcoM-3ZOO simulation. It now falls into the range of satellite-based observations (35–70 Pg C y^{-1}, Carr et al., 2006) and gets closer to the recent estimate of 48.7 Pg C y^{-1} to 52.5 Pg C y^{-1} (Kulk et al., 2021). In addition, the ratio of EP to NPP decreases from 17% to 12% illustrating the altered carbon pathways in the model.

In REcoM-3ZOO, the small phytoplankton is spread across the global ocean, while the diatom functional type mainly dominates in high latitudes and in the Equatorial Pacific (Figure 2) due to the growth limitation by silicic acid (Smetacek, 1998). The distribution of the zPFTs shows distinct spatial patterns. While microzooplankton

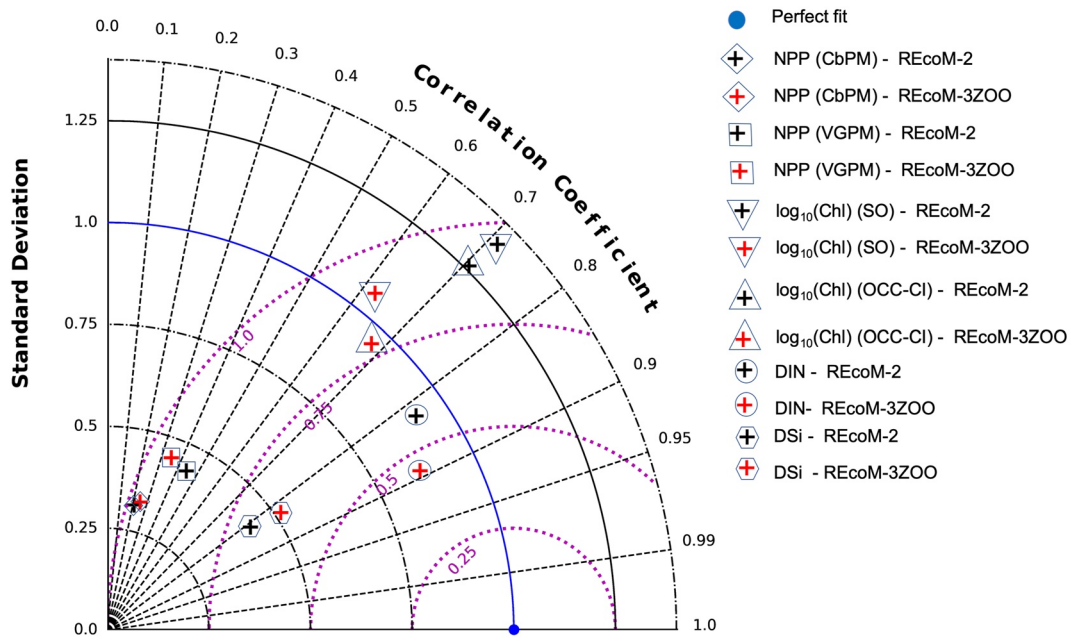

Figure 3. Normalized Taylor diagram comparing the distributions of surface concentration in annual mean chlorophyll (log_{10}(Chl), mg m^{-3}), dissolved inorganic nitrogen (DIN, mmol m^{-3}), silicic acid (DSi, mmol m^{-3}) and net primary production (NPP, mg C m^{-2}) for REcoM-2 (in black) and REcoM-3ZOO (in red) with observations. Pink dotted lines show the axes for the root mean square error (RMSE). Surface chlorophyll observations are taken from OC-CCI (Sathyendranath et al., 2019) for global and from Johnson et al. (2013) for the Southern Ocean (SO) comparison. World Ocean Atlas 2018 products (Garcia et al., 2018) are used for nutrient observations. Net primary production observations are taken from the VGPM Behrenfeld and Falkowski (1997) and CBPM Westberry et al. (2008) data sets. The blue dot shows the perfect fit.

is widely spread in the global ocean, in line with Buitenhuis et al. (2010), mesozooplankton is mainly present in subpolar areas and in the Equatorial Pacific in accord with observational data compilations (Moriarty & O'Brien, 2013). The macrozooplankton group is mainly represented in the polar regions, in agreement with the reported global macrozooplankton data set (Moriarty et al., 2013). Microzooplankton biomass has a minimum in subtropical gyres. This is in agreement with previous modeling studies (Buitenhuis et al., 2010; Le Quéré et al., 2016), and we relate this to the minimum in phytoplankton biomass as food source and the underrepresentation of picophytoplankton and nitrogen fixers in our mixed small phytoplankton functional group.

3.2. Comparison of the Global Nutrient and Chlorophyll Concentrations in REcoM-2 and REcoM-3ZOO

The overall differences in how well REcoM-2 and REcoM-3ZOO agree with climatological data for chlorophyll, NPP and nutrients are quantified statistically in a Taylor diagram (Taylor, 2001). The differences in correlation coefficients with observational data sets are less than 0.1 between the two simulations (Figure 3). The correlation coefficients are slightly lower with 0.35 for annual mean chlorophyll, and 0.67 for NPP. In REcoM-3ZOO, the correlation coefficients are slightly higher with 0.89 for annual mean DIN and 0.83 for silicic acid concentrations. In addition, the normalized standard deviation is closer to the observations and root mean square error smaller for annual mean chlorophyll concentrations in REcoM-3ZOO. Both model versions generally produce similar spatial patterns of surface nutrient and chlorophyll concentrations (Figures 4 and 5). A notable exception is the South Pacific, where a strong change in surface DIN and iron concentration occurs.

Observed surface annual mean DIN and silicic acid concentrations are higher in the high latitudes and Equatorial Pacific compared to the rest of the ocean (Figure 4). Both model versions also produce a similar spatial distribution of nutrients compared to WOA18 products (Garcia et al., 2018). However, while REcoM-2 has a strong positive bias in surface DIN concentrations in the South Pacific (20°S–40°S), the bias decreases significantly in REcoM-3ZOO. The mean DIN concentration decreases from 7 mmol m^{-3} in REcoM-2 to 2.2 mmol m^{-3} in REcoM-3ZOO and gets closer to observations (0.8 mmol m^{-3}) in the South Pacific. We find that this is

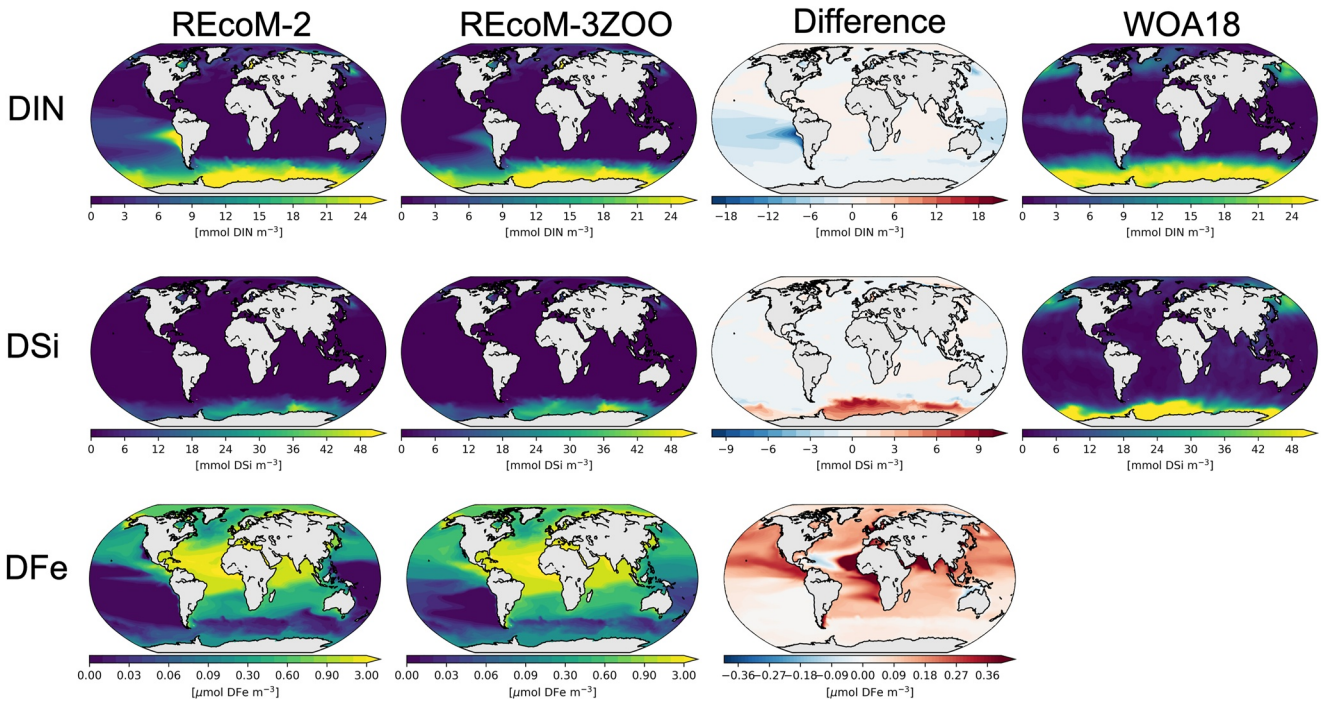

Figure 4. Annual mean surface nutrient concentrations (dissolved inorganic nitrogen (DIN), silicic acid (DSi), dissolved iron (DFe)) in REcoM-2, REcoM-3ZOO, difference (REcoM-3ZOO minus REcoM-2) and WOA18 (Garcia et al., 2018). Model results are averaged over the last 5 years of the simulation.

related to the more complex ecosystem interactions, which include different pathways of nutrient recycling by zooplankton. In addition, the mean DIN concentrations decrease in northern and southern high latitudes. In the northern high latitudes, the mean surface DIN concentrations (4.1 mmol m^{-3} in REcoM-2 and 3.5 mmol m^{-3} in REcoM-3ZOO) are lower than the observations (5.6 mmol m^{-3}). In the southern high latitudes, mean DIN concentrations also slightly decrease from 19.9 mmol m^{-3} in REcoM-2 to 19.0 mmol m^{-3} in REcoM-3ZOO. Both model versions underestimate the surface mean silicic acid concentrations in the high latitudes. This bias is ameliorated in REcoM-3ZOO with a DSi concentration increase by 20% to 15 mmol m^{-3} south of 50°S getting closer to observations (31.6 mmol m^{-3}). The annual mean iron concentration increases in REcoM-3ZOO by 20%–25% in high latitudes and by 270% (from 0.04 μmol m^{-3} to 0.14 μmol m^{-3}) in the South Pacific compared to REcoM-2. In the South Pacific, the area where iron is the most limiting nutrient shrinks in REcoM-3ZOO compared to REcoM-2 (Figure S5 in Supporting Information S1). This is an important feature, since it clearly improves the surface chlorophyll concentrations (Figure 5).

The new zooplankton formulation affects the surface mean chlorophyll concentrations directly by grazing pressure and indirectly by altered nutrient availability. The spatial distributions of surface chlorophyll of both simulations resemble each other with the highest chlorophyll concentrations in high latitudes and the Equatorial Pacific

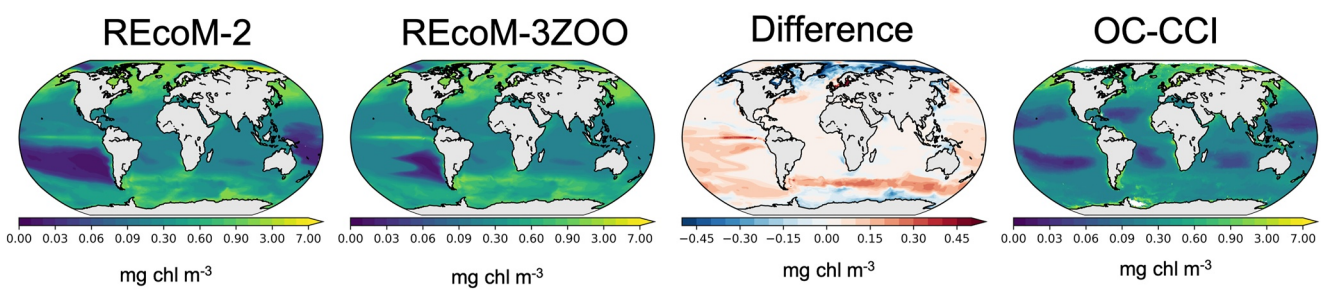

Figure 5. Annual mean surface chlorophyll concentrations in REcoM-2, REcoM-3ZOO, their difference (REcoM-3ZOO minus REcoM-2) and OC-CCI satellite product (OC-CCI, Sathyendranath et al., 2019). Model results are averaged over the last 5 years of the simulation.

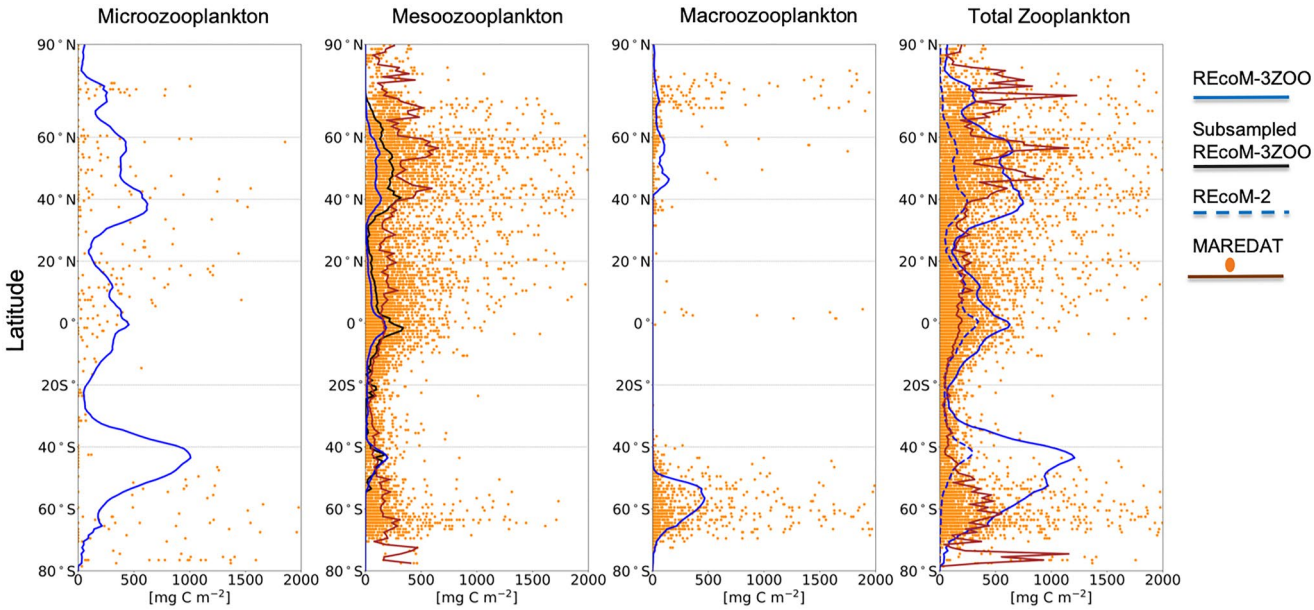

Figure 6. Zonally and annually averaged and depth-integrated zooplankton biomass (micro-, meso-, and macrozooplankton, total zooplankton) in REcoM-2 and REcoM-3ZOO compared to annually averaged and depth-integrated gridded MAREDAT observations (orange dots, Buitenhuis et al., 2010; Moriarty & O'Brien, 2013; Moriarty et al., 2013). The dark brown line shows the zonal average of MAREDAT observations. The blue lines denote the zonal average of zooplankton in REcoM-3ZOO and the black line shows the zonal average zooplankton from the model subsampled for the grid points where data is available. Similarly, the dashed blue line shows the average of zooplankton in REcoM-2. The data for micro- and macrozooplankton are too sparse to calculate a zonal mean of the subsampled model.

(Figure 5). In REcoM-3ZOO, a previously apparent strong positive bias in the North Atlantic and the Arctic chlorophyll disappears. In these regions, the annual mean chlorophyll concentrations decrease from 1.2 mg m^{-3} to 0.94 mg m^{-3}, in better agreement with the remotely sensed 0.9 mg m^{-3} (Figures 5 and 6). South of 50°S, the mean chlorophyll concentration remains similar with 0.55 mg m^{-3} in REcoM-2 and 0.57 mg m^{-3} in REcoM-3ZOO, close to satellite observations (0.63 mg m^{-3}, Johnson et al., 2013). In the Atlantic and Indian sectors of the Southern Ocean, the increase of chlorophyll can reach up to 0.58 mg m^{-3} in REcoM-3ZOO. Newly distributed iron and nitrate concentrations in the South Pacific provide a noticeable improvement in the mean surface chlorophyll concentrations. The mean value increases in the South Pacific from 0.05 mg m^{-3} in REcoM-2 to 0.12 mg m^{-3} in REcoM-3ZOO and matches better with satellite observations of 0.1 mg m^{-3} (Sathyendranath et al., 2019).

3.3. Grazing and Nutrient Recycling by Zooplankton

Figure 6 shows the zonally and annually averaged and depth-integrated zooplankton biomass in the model and a comparison with data compilations. We use three MAREDAT data compilations for microzooplankton (Buitenhuis et al., 2010), mesozooplankton (Moriarty & O'Brien, 2013) and macrozooplankton biomass (Moriarty et al., 2013). In REcoM-3ZOO, the zonal average of zooplankton biomass follows a similar distribution as apparent in the MAREDAT data set (Figure 6). While microzooplankton and mesozooplankton prevail from north to south with maxima in the subpolar and equatorial regions, macrozooplankton is primarily present in the higher latitudes. The modeled mesozooplankton biomass reproduces the latitudinal pattern from the data, although the modeled zonal mean is on the low side. This is especially true in subpolar and polar regions, but can be partly explained by sparse sampling in the northern hemisphere (compare full and subsampled model in Figure 6). The total zooplankton biomass is higher in REcoM-3ZOO compared to REcoM-2. While total zooplankton biomass increases throughout all latitudes, the strongest increase occurs poleward of 30°N and 30°S (Figure 6). Maxima in annually averaged and depth-integrated total zooplankton biomass can reach up to 2000 mg C m^{-2} in MAREDAT in the high latitudes. In REcoM-3ZOO, the maximum of total zooplankton biomass increases from 783 mg C m^{-2} in REcoM-2 to 2877 mg C m^{-2}. The zonally averaged total zooplankton biomass is almost 0 mg C m^{-2} poleward of 60°N and 60°S in REcoM-2. It increases to 1339 mg C m^{-2} north of 60°N and to 577 mg C m^{-2} south of 60°S in REcoM-3ZOO.

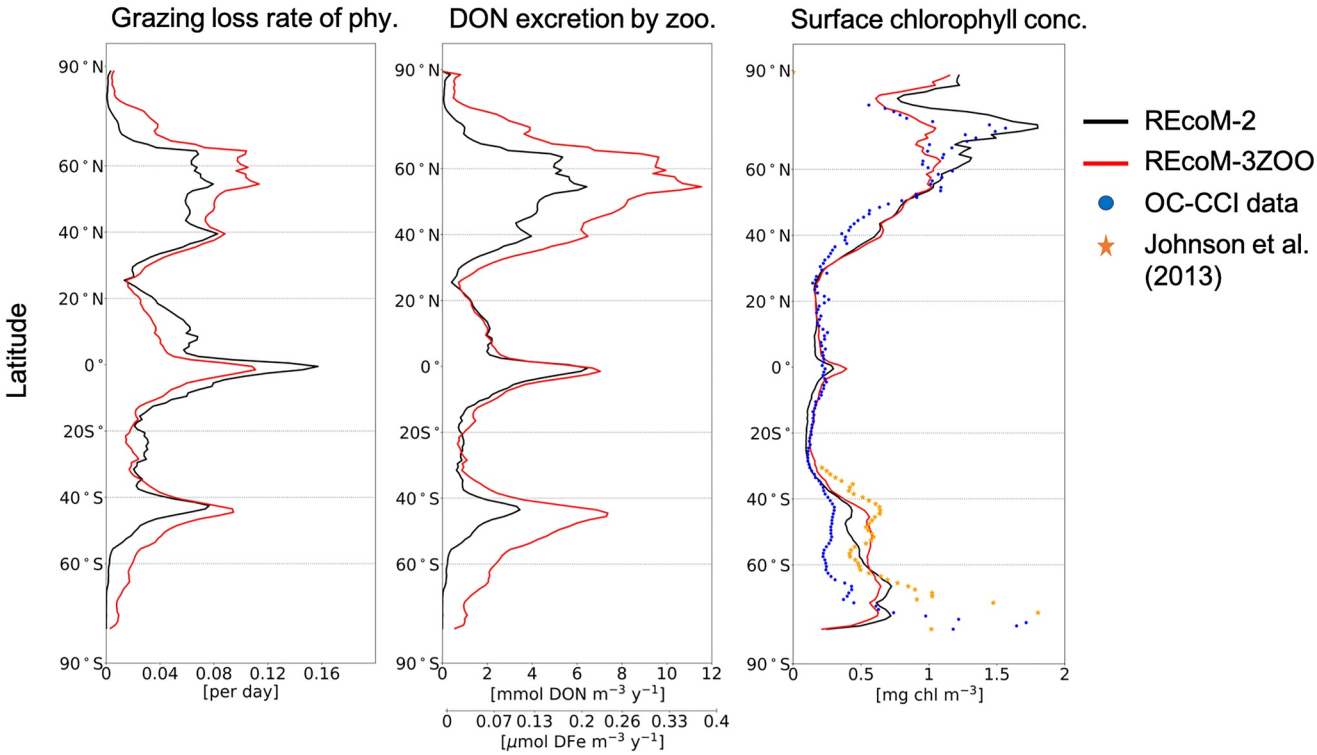

Figure 7. Annual mean surface grazing loss of phytoplankton, zooplankton excretion of dissolved organic nitrogen (DON) and chlorophyll concentrations in REcoM-2 (black) and REcoM-3ZOO (red). Surface chlorophyll concentrations from satellite products are shown as blue dots (Sathyendranath et al., 2019) and orange stars (Johnson et al., 2013).

These changes in zooplankton biomass and distribution affect grazing patterns and the fast recycling of nutrients by zooplankton excretion. Consequently, they impact the nutrient fields presented in Section 3.2. We observe a distinct latitudinal pattern with an increased grazing loss of phytoplankton in the extra-tropics and a reduced grazing loss in the tropics in the new parametrization in REcoM-3ZOO (Figure 7). In REcoM-2, the highest annual mean grazing-related phytoplankton loss in the global ocean occurs between 20°N and 20°S, which is a result of the temperature-dependence of grazing. The gradient between phytoplankton loss rates in high latitudes and in the tropics is smaller in REcoM-3ZOO compared to REcoM-2, as a result of the parametrization of zPFTs with different parameter values of excretion and grazing and temperature dependencies. In REcoM-3ZOO, the spatial peak of the grazing loss of phytoplankton occurs between 40°N and 60°N (Figure 7, Table 3). In the subtropics (20°–40°N, 20°–40°S), the zooplankton-related grazing loss of phytoplankton remains similar in both simulations (0.033–0.021 d^{-1} in REcoM-2, 0.037–0.020 d^{-1} in REcoM-3ZOO). In the northern temperate (40°–60°N) and high latitudes (60°–90°N), the grazing loss of phytoplankton increases by 26% and 120%, respectively in REcoM-3ZOO. Consequently, this decreases the mean surface chlorophyll concentrations by 32% and satellite-based (1.02 mg chl m^{-3}) and model-based (0.91 mg chl m^{-3}) estimates come to close agreement. In the southern hemisphere temperate and high latitudes (40°–60°S, 60°–90°S), a similar increase in grazing loss rates occurs, ranging between 100% (40°–60°S), and 1800% south of 60°S where grazing rates were previously very small. Despite this strong grazing loss, we see a 20% increase in mean chlorophyll concentrations (40°–60°S), which we relate to the nutrient excretion of zooplankton.

DON and with it DFe excretion intensifies throughout the ocean (Figure 7) with a notably larger increase outside the tropics (poleward of about 30°N and S). Local exceptions occur in the Equatorial Pacific and some coastal regions (e.g., off the coast of Australia, Figure 8). The increase of excretion rates is expected since the rates are directly coupled to the total zooplankton biomass in the model. DON and DFe excretion rates have identical spatial patterns as the DFe excretion rate is calculated by multiplication of the DON excretion rate with a fixed Fe:N ratio in the model. While the annual mean DON excretion by zooplankton is 1.61 mmol m^{-3} y^{-1} in REcoM-2 between 40°S and 60°S, it is 5.55 mmol m^{-3} y^{-1} in REcoM-3ZOO. An increase of DFe excretion

Table 3
Annual Mean Phytoplankton Grazing Loss Rate (d^{-1}), Dissolved Organic Nitrogen (DON) (mmol DON m^{-3} y^{-1}) and DFe (μmol DFe m^{-3} y^{-1}) Excretion by Zooplankton, Surface Chlorophyll Concentrations (mg Chl m^{-3}) in REcoM-2 and REcoM-3ZOO Averaged Over the Last Five Years of the Simulation in Seven Latitudinal Bands

	Grazing loss rate		DON excretion by zoo.		DFe excretion by zoo.		Surface chlorophyll conc.		
Region	REcoM-2	REcoM-3ZOO	REcoM-2	REcoM-3ZOO	REcoM-2	REcoM-3ZOO	REcoM-2	REcoM-3ZOO	Satellite
60°–90°N	0.02	0.04	1.55	4.02	0.05	0.13	1.34	0.91	1.02
40°–60°N	0.07	0.08	4.44	8.13	0.14	0.27	0.81	0.81	0.7
20°–40°N	0.03	0.03	1.39	2.32	0.05	0.08	0.27	0.29	0.23
20°N–20°S	0.06	0.04	2.34	2.63	0.08	0.09	0.16	0.20	0.2
20°–40°S	0.02	0.02	0.92	1.33	0.03	0.04	0.16	0.20	0.16
40°–60°S	0.03	0.05	1.61	4.80	0.05	0.16	0.43	0.54	0.27 (0.52)
60°–90°S	<0.01	0.01	0.11	1.76	<0.01	0.05	0.65	0.6	0.3 (0.83)

Note. The last column shows the satellite-based estimates of surface chlorophyll concentrations from OC-CCI (Sathyendranath et al., 2019) and in parentheses from Johnson et al. (2013).

occurs in the same region, between 40°S and 60°S. The zooplankton DFe excretion is 0.05 μmol m^{-3} y^{-1} in REcoM-2, and increases to 0.16 μmol m^{-3} y^{-1} (Figure 3).

In summary, we relate the reduced chlorophyll bias in the North Atlantic and the Arctic to higher grazing-related phytoplankton loss terms. Considering the role of iron limitation in the Southern Ocean, we conclude that here the nutrient recycling through zooplankton has a stronger effect on mean chlorophyll concentrations than grazing. The increase in nutrients and chlorophyll in the Equatorial Pacific (Figures 4 and 5) and in the Southern Ocean (iron) are co-located with regions of strongest change in nutrient excretion.

3.4. Competing Effects of Phytoplankton Grazing Loss and Nutrient Excretion by Zooplankton

Grazing loss of phytoplankton and nutrient excretion by zooplankton show spatial patterns in the model that are directly coupled with zooplankton biomass. In REcoM-2, the annual mean grazing loss of phytoplankton is 0.22 d^{-1} in the Equatorial Pacific, around 0.07 d^{-1} in the North Atlantic and coastal regions, and <0.01 d^{-1} south

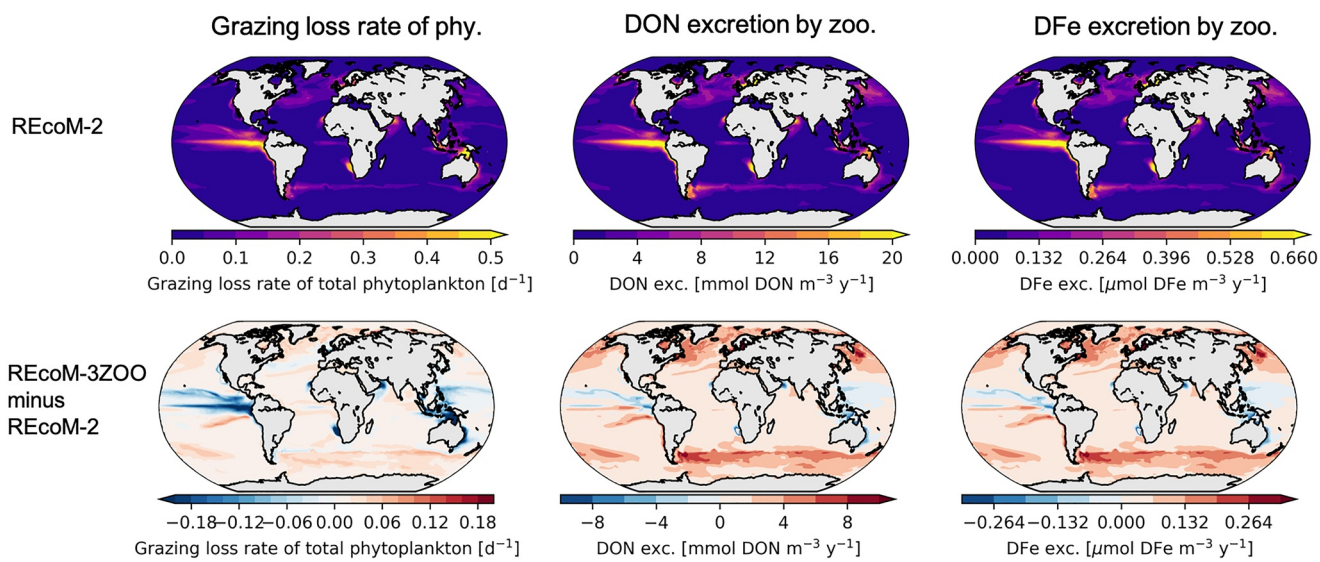

Figure 8. Annual mean phytoplankton loss rate due to zooplankton grazing (d^{-1}), dissolved organic nitrogen (DON) (mmol m^{-3} y^{-1}) and DFe (μmol m^{-3} y^{-1}) excretion by zooplankton in REcoM-2 and the change in REcoM-3ZOO (REcoM-3ZOO minus REcoM-2). The model results are averaged over the last 5 years of the simulations.

of 50°S (Figure 8). While both processes play only a minor role in the high latitudes in REcoM-2, they become an important component for the ecosystem dynamics in REcoM-3ZOO (Figure 8). The annual mean grazing loss of phytoplankton increases by 28% (from 0.07 d^{-1} to 0.09 d^{-1}) in the North Atlantic, and by more than 100% (from <0.01 d^{-1} to 0.02 d^{-1}) in the Southern Ocean. One exceptional region is the Equatorial Pacific where the average grazing loss of phytoplankton decreases by 50% (from 0.3 d^{-1} to 0.15 d^{-1}, Figure 8). We relate this to the differences of the food web structure in the two model versions. While a single herbivorous zooplankton increases its grazing at warmer temperatures and high food abundance in REcoM-2, feeding pressure of mesozooplankton keeps microzooplankton in check and thus decreases the grazing pressure of microzooplankton on phytoplankton. The nutrient excretion by zooplankton increases throughout the global ocean since total zooplankton biomass increased in REcoM-3ZOO (Figure 6), but the magnitude is largest in temperate and high latitudes (poleward of 40°N/S). The annual mean of DON excretion increases by 86% (from 4.2 to 7.8 mmol DON m^{-3} y^{-1}) in the North Atlantic and by more than 100% (from 0.39 to 2.66 mmol DON m^{-3} y^{-1}) in the Southern Ocean, respectively.

Overall, a reinforcement or decline of the same patterns in grazing and nutrient excretion with similar seasonal patterns occurs north of 50°S (Figure S1 in Supporting Information S1). However, a substantial change in zooplankton-related processes appears south of 50°S in the simulation with REcoM-3ZOO. The grazing loss of phytoplankton reaches 0.2 d^{-1} in spring and summer, whereas it was barely existent in REcoM-2. A similar effect can be observed in DON excretion (followed by iron excretion), reaching up to 3 mmol DON m^{-3} per month in November. Zooplankton nutrient excretion between January and April increases the chlorophyll concentrations in the Southern Ocean in the same period (Figure 11), but we have so far not investigated the direct effect on phytoplankton phenology.

Although we use the same ingestion function for zooplankton in both model versions, temperature dependencies and the parameter values differ. In the original version REcoM-2, the grazing rate constant of zooplankton is 2.4 d^{-1} at 15°C that increases up to 5 d^{-1} at 30°C and the assimilation efficiency is 0.4 (the remaining 60% of grazing are routed to fecal pellet production and sloppy feeding). This parametrization causes first a very high grazing rate in warm equatorial regions and consequently a strong annual grazing loss rate of phytoplankton (Table 3, Figure 7). Second, this leads to low zooplankton biomass in the cold polar regions and therefore causes grazing loss rates for phytoplankton and nutrient excretion by zooplankton to be very low (Table 3, Figure 7). In REcoM-3ZOO, parametrizing three zPFTs gives the flexibility to choose different assimilation efficiencies and temperature dependencies of grazing. For example, the microzooplankton temperature-dependent grazing rate is higher than for mesozooplankton. The initial assimilation efficiency of the mesozooplankton group is 0.8 and decreases with increasing prey abundance. Also, polar slow-growing macrozooplankton which is parametrized as krill (Karakuş et al., 2021) is represented in this version. This new parameterization allows us to improve the spatial distribution of zooplankton biomass and related processes in high latitudes (Figure 8). Figure 9 shows the point-wise comparison of zooplankton biomass, nutrient excretion and grazing rates as well as grazing loss of phytoplankton with annual mean surface temperature. As we showed in previous sections, the total zooplankton biomass increases in all three subregions (40–90°, 40–40°S and 40–90°S) in REcoM-3ZOO. The maximum of zooplankton biomass is three times higher in REcoM-3ZOO and the strongest increase occurs at temperatures below 14°C. These changes in biomass directly affect the DON excretion and grazing rate of zooplankton which consequently all increase. Grazing and nutrient excretion follow the change in biomass. The magnitude of DON excretion and grazing by zooplankton is similar in both model versions at temperatures above 14°C, and increases at colder temperatures in REcoM-3ZOO because this is where we see the largest zooplankton biomass increase. The grazing loss of phytoplankton is a balance between the positive effects of more DON excretion and the negative effect of higher zooplankton grazing. Poleward of 40°N/S, phytoplankton grazing loss clusters above and below the 1:1 line, but on average the grazing loss of phytoplankton increases by 100% (from 0.02 to 0.04 d^{-1}) poleward of 40°S and by 40% (from 0.05 to 0.07 d^{-1}) poleward of 40°N in REcoM-3ZOO. However, between 40°S and 40°N the phytoplankton loss is up to three times lower in REcoM-3ZOO as a result of the new model state with a higher phytoplankton biomass. Our results demonstrate that a high zooplankton biomass does not directly imply a high grazing loss of phytoplankton in biogeochemical models. The loss term results from an interplay of temperature dependency, chosen parameter values for grazing and excretion rates, and food web structure in the model.

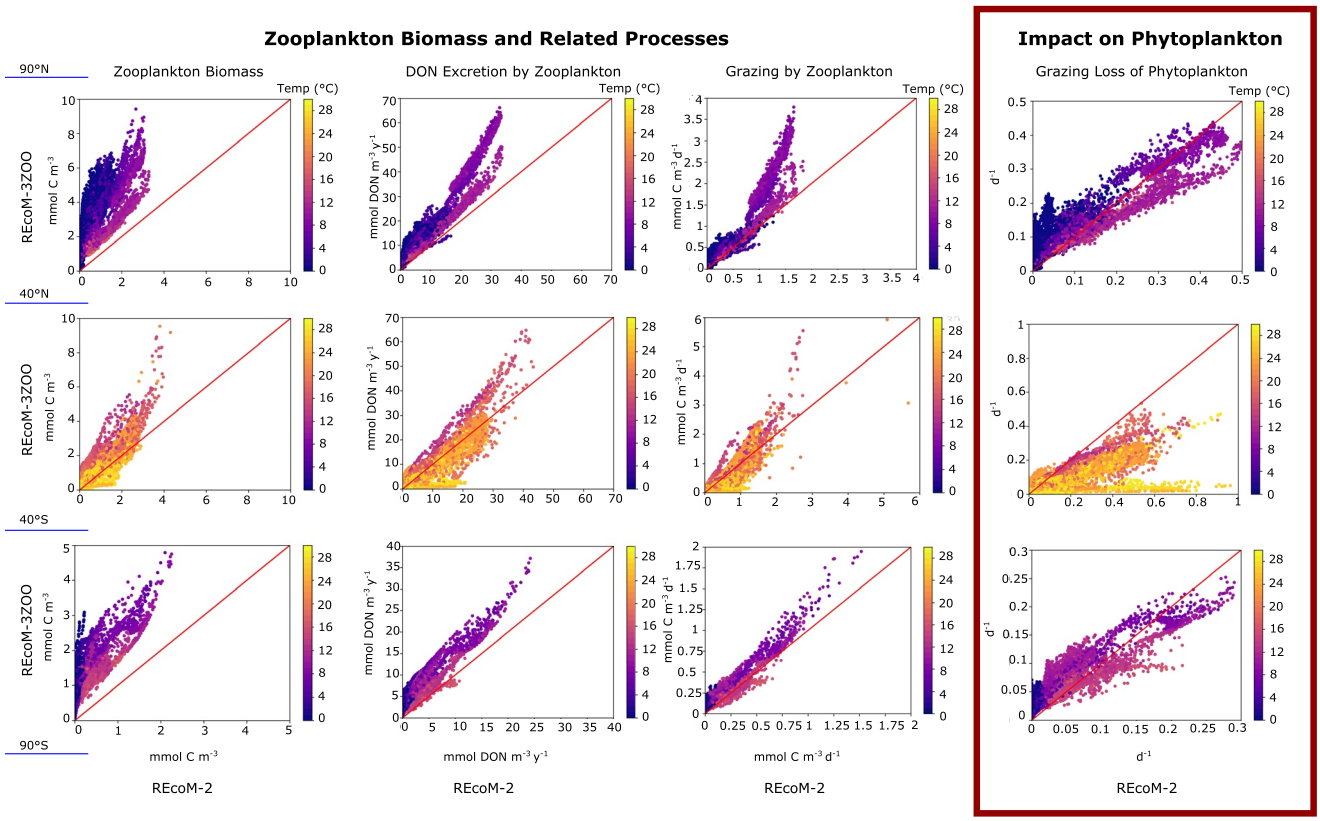

Figure 9. Point-wise comparison of annual mean surface zooplankton biomass (mmol C m^{-3}), dissolved organic nitrogen (DON) excretion by zooplankton (mmol m^{-3} y^{-1}), grazing by zooplankton (mmol C m^{-3} d^{-1}) and grazing loss of phytoplankton (d^{-1}) between REcoM-2 (*x*-axis) and REcoM-3ZOO (*y*-axis) in three regions from north to south (90°–40°N, 40°N–40°S and 40°–90°S). Each dot represents one surface model grid point. The red line represents the one-to-one line in the plots. The color shading indicates the annual mean surface temperature. Note the different *y*-axis ranges.

3.5. Impact of Zooplankton Grazing on Southern Ocean Phytoplankton Bloom Phenology

Phytoplankton bloom start and peak days occur later in the year in the whole Southern Ocean south of 50°S in REcoM-3ZOO (Figure S3 in Supporting Information S1). However, the magnitude of the effect is larger in regions where high zooplankton biomass causes larger grazing loss of phytoplankton. In this section, we focus on a specific region in the Southern Ocean (subpolar Atlantic sector of the Southern Ocean, 50°–60°S and 20°E−60°W) to analyze the impact of the zooplankton parametrization on phytoplankton phenology. We specifically chose this region since it is located in an area of substantial change in zooplankton processes from REcoM-2 to REcoM-3ZOO.

We start the analysis of phytoplankton bloom phenology with the carbon accumulation rate-based analysis. As we showed in the previous sections, the ecosystem structure of the two model versions differs. Therefore, we describe the bloom phenology separately in each model version rather than comparing the two simulations directly.

In REcoM-2, the onset of the phytoplankton bloom (the day when the biomass accumulation rate becomes positive) happens in the last week of July, that is, after the winter solstice and when deepening of the mixed layer occurs (Figures 10a and 10c). The maximum carbon accumulation rate of the phytoplankton biomass (climax) occurs in the last week of October when the MLD is roughly halfway between its deepest and shallowest state and can be related to light availability. Maximum phytoplankton biomass (apex) falls into the first week of November with only 11 days between climax and apex. Phytoplankton reaches its maximum biomass shortly after the carbon accumulation rate is at its maximum. Phytoplankton loss rates due to grazing are very low compared to other loss rates (Figures 10c and 10e). We interpret this as a sign of a too weak representation of zooplankton grazing in REcoM-2. Both phytoplankton groups, small phytoplankton and diatoms, are iron-limited, but the limitation is stronger for diatoms (Figure 10g).

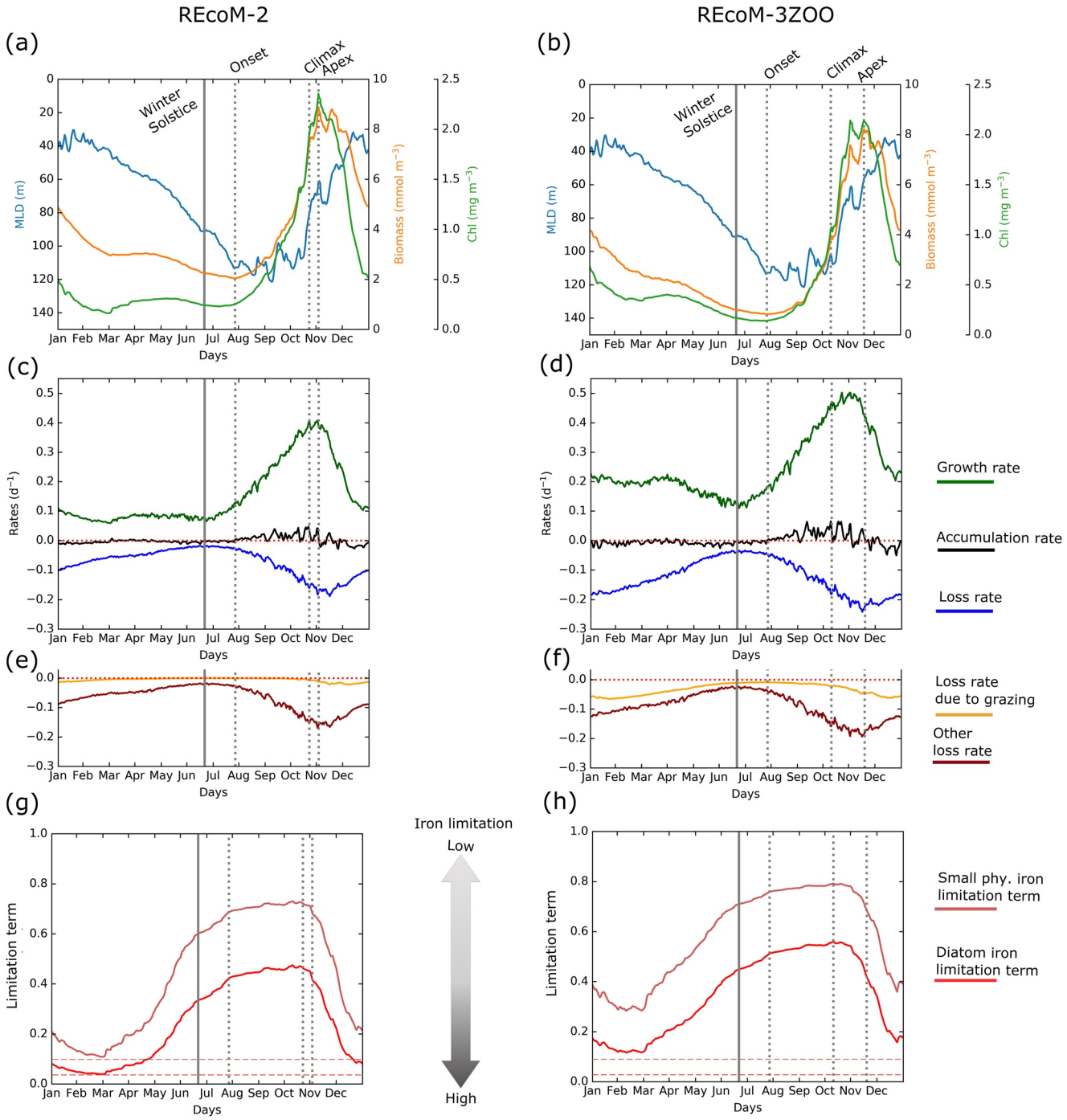

Figure 10. Seasonal cycles of mixed layer depth (MLD), surface chlorophyll, phytoplankton biomass, growth and loss rates in REcoM-2 (left) and REcoM-3ZOO (right) (a, b) Mixed layer depth (blue), phytoplankton biomass (orange) and chlorophyll (green) (c, d) Growth rate (green), net accumulation rate (black), and loss rates (blue) of phytoplankton (e, f) Decomposition of phytoplankton loss rates into loss rate due to grazing (orange) and other loss rates (aggregation, respiration, excretion; dark red) (g, h) Iron limitation term affecting phytoplankton growth and horizontal lines show the minimum of the limitation term in REcoM-2 for both phytoplankton groups. Bloom onset, climax, and apex days are indicated as vertical dashed lines. The seasonal cycle was calculated as the average over the last 5 years of the simulation, from daily model output.

In REcoM-3ZOO, the phytoplankton bloom onset happens in the last week of July as in REcoM-2. The climax, however, now occurs in the first week of October, before significant shoaling of the MLD sets in (Figures 10b and 10d). This can be explained by the dilution of zooplankton when MLD is at its maximum (Behrenfeld et al., 2013) and is supported by the fact that phytoplankton losses due to zooplankton grazing are now an

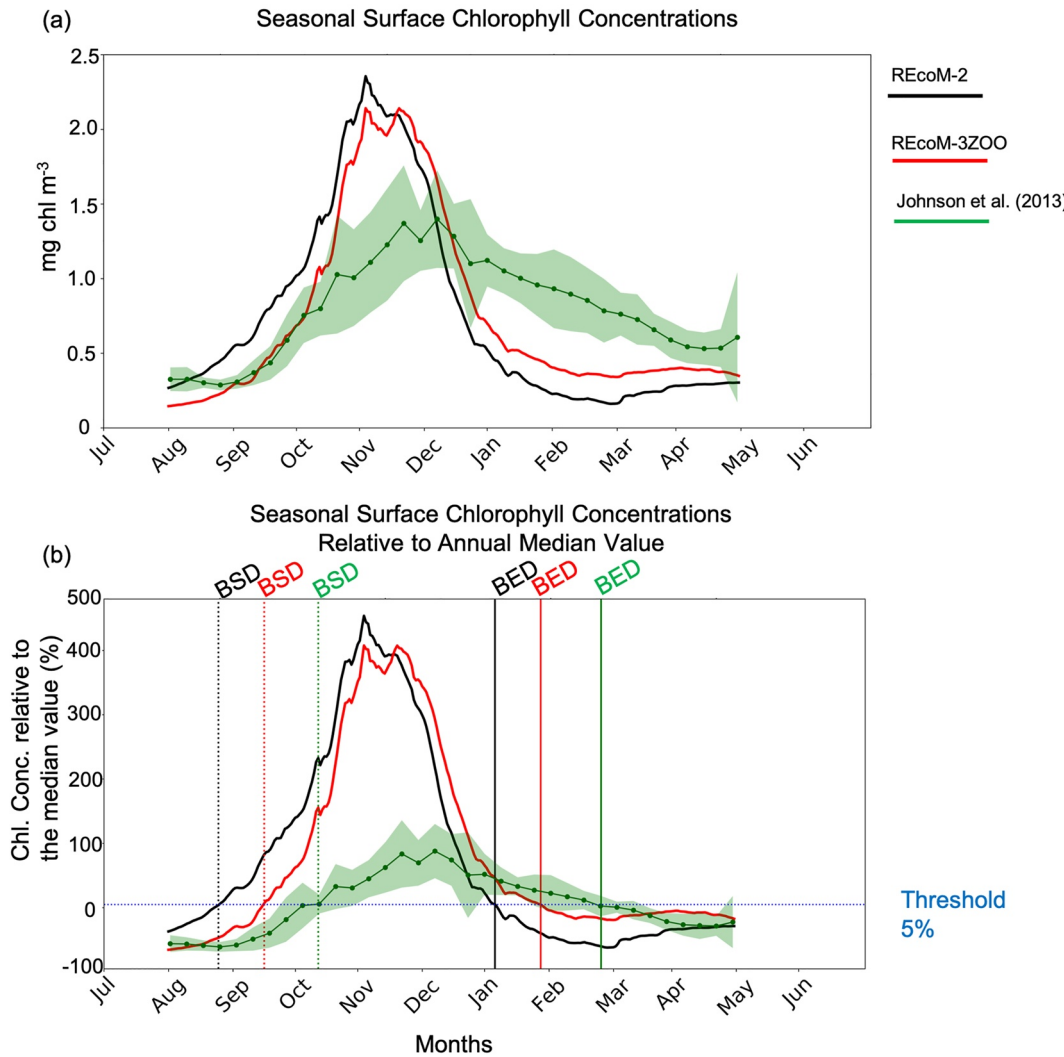

Figure 11. Comparison of the seasonal cycle of phytoplankton chlorophyll concentrations in two simulations and in a satellite product (2003–2012, Johnson et al., 2013). The seasonal cycle was calculated as the average over the last 5 years of the simulations, from the daily model output. (a) Seasonal surface chlorophyll concentrations, (b) seasonal surface chlorophyll concentrations relative to the annual median value. The horizontal blue line represents the 5% threshold. The vertical dashed lines are the mean bloom start days (BSD) in REcoM-2 (black), REcoM-3ZOO (red) and in the satellite product (green). Bloom end days (BED) are shown with the solid lines with the same color code.

important component of mortality losses (Figure 10f). Total zooplankton grazing contributes up to 39% to spring and summer phytoplankton loss rates. The time that passes between climax and apex is 29 days because phytoplankton biomass accumulation is delayed by stronger grazing pressure. In REcoM-3ZOO, iron limitation is lower than in the original version of the model (Figure 10h).

The results of the two simulations illustrate the sensitivity of the phytoplankton bloom phenology to modeled ecosystem structure and processes in the biogeochemical model. Both model versions can produce the main properties of phytoplankton growth (e.g., high rates in spring) depending on abiotic factors (light, temperature etc.). However, a detailed analysis reveals differences. Shifts in the timing of the climax between the model versions, for example, show that the representation of zooplankton processes can lead to a different system state, in which carbon accumulation is driven by grazer dilution rather than by light limitation (bottom-up control).

We present next the chlorophyll-based analysis and comparison with satellite data. In REcoM-2, the BSD occurs in August (day 237) and bloom peak is in November (day 306, Figure 11). We see a sharp decrease in chlorophyll

concentration after the peak, and the bloom terminates in the beginning of January (day 6). The mean chlorophyll concentration is 0.26 mg chl m^{-3} between January and May.

The BSD occurs in September (day 258) in REcoM-3ZOO, which is three weeks later than in REcoM-2, whereas the peak day remains unchanged (day 306 in both simulations, Figure 11). The peak of chlorophyll occurs as a plateau and lasts 2 weeks longer in the simulation with three zooplankton groups (until day 322). Also, the shift in the BSD and the increase in summer chlorophyll concentrations (due to the fast recycling of nutrients) move the BED by 3 weeks (to day 27). The calculated bloom duration (time between BSD and BED) is similar in REcoM-3ZOO. We caution that this should not be interpreted as no change of the bloom duration in REcoM-3ZOO, as the result of the threshold method is strongly dependent on the chosen threshold value. In REcoM-3ZOO simulations, the chlorophyll concentrations after the BED are very close to the threshold (until May). The mean chlorophyll concentration is 0.42 mg chl m^{-3} between January and May which is almost two times higher than in REcoM-2.

In each year of the satellite observations, chlorophyll concentrations reach the 5% threshold value after mid-September (bloom start), reach peak chlorophyll between October and December (up to 200% of the annual median) and slowly decline from 100% to 0% until mid-March (Figure 11b). In the average over 10 years, the satellite-derived bloom starts in October (day 291) and ends in February (day 33, marked green BSD and BED, Figure 11b). Even though there are certain limitations to using the satellite products (missing areas, clouds, interannual variability) for comparison, the start of bloom occurs consistently after mid-September and the end of bloom consistently until mid-March in all years. With the more complex parametrization of zooplankton in REcoM-3ZOO, the phenology indicators compare better with the satellite-derived indicators than in REcoM-2. Specifically, the very early bloom start date in August in REcoM-2 is delayed to mid-September, and also the bloom end date shifts from early January in REcoM-2 to the end of January in REcoM-3ZOO (Figure 11b).

Our results indicate that zooplankton grazing delays the bloom initiation and controls the peak of the bloom. Macrozooplankton grazing is an important component of phytoplankton loss rate throughout the year (Figure S2 in Supporting Information S1). Despite exerting the highest grazing pressure of all zooplankton groups between the winter solstice and bloom onset, the day of bloom onset remains the same in the two model versions (Figure 10). Micro- and mesozooplankton biomass and consequently grazing follow the seasonal cycle of phytoplankton very closely. Therefore, their contributions to phytoplankton loss rates are higher, especially in spring and summer (Figure S2 in Supporting Information S1). Both, but especially the more abundant microzooplankton, control the spring and summer chlorophyll concentrations and phytoplankton biomass in the model.

We identify two distinct roles of zooplankton in the simulated phytoplankton phenology. First, zooplankton affects the duration of the period between climax and apex. Zooplankton grazing prolongs this phase by controlling the magnitude of the spring peak of biomass and chlorophyll concentrations (Figure 10a). Second, zooplankton prolongs the growing season (apex occurs later) and sustains higher chlorophyll concentrations in summer and autumn (after apex) due to fast nutrient recycling (Figure 11a).

4. Discussion

4.1. The Role of Zooplankton in Nutrient Recycling

Zooplankton grazing is known to be an important phytoplankton loss term that can exert a dominant control over phytoplankton dynamics (Prowe et al., 2012). However, zooplankton does not only affect phytoplankton biomass by grazing, but also by recycling of nutrients such as iron and nitrogen (Alcaraz et al., 2010; Tovar-Sanchez et al., 2007). A portion of the assimilated organic carbon and nitrogen by zooplankton is released as DOM (Møller, 2007; Saba et al., 2009) and comprises an important share of total DOM release (7%–80%, Carlson & Hansell, 2015). In our simulation, the added nutrient recycling leads to an increase of global NPP by 25% (Table 2). Representing a more complex and realistic grazing and nutrient recycling by zooplankton decreases the biases in nutrient and chlorophyll concentrations (Figures 4 and 5). Our analysis emphasizes that zooplankton nutrient recycling increases summer chlorophyll concentrations in the Southern Ocean (Figure 11a) and affects bloom phenology (discussed in Section 4.2). Therefore, our results emphasize the importance of a mechanistic representation of the zooplankton compartment in ocean biogeochemical models.

Zooplankton herbivory partitions the primary production between zooplankton growth, export, and recycled production. Although the global NPP increases substantially by 7.7 Pg C y^{-1} (25%) to 38 Pg C y^{-1} due to nutrient recycling by zooplankton after the parametrization of zPFTs, the total export decreases by 0.5 Pg C y^{-1} (10%) to 4.7 Pg C y^{-1}. Consequently, the export ratio of the modeled ecosystem decreases. This suggests that more carbon and nutrients are retained in the euphotic zone after a more realistic food web representation.

Pathways for nutrient recycling by zooplankton are sloppy feeding, excretory release, and leaching from fecal pellets (Carlson & Hansell, 2015). The relative contributions of these different processes and the biological availability of recycled nutrients vary largely, depending on zooplankton body mass and temperature (Ikeda, 2014), food quality (Saba et al., 2009), prey size (Møller, 2007) or species (Böckmann et al., 2021). In this study, we only consider the effect of total zooplankton biomass and indirectly of temperature (since temperature affects zooplankton grazing and consequently biomass) on nutrient excretion rates. While our results clearly suggest that the zooplankton compartment is more than a top closure term in biogeochemical models, we are only starting to resolve the relevant processes. Further work is required to represent the role of zooplankton for nutrient recycling based on mechanistic process understanding such as effects of food type and quality, prey size, and different species.

In our simulations, micronutrient (iron) recycling emerged as a determining process in the Southern Ocean (Figure 10h). The increased iron availability fuels the phytoplankton growth throughout the year (Figure 10d). In particular, total chlorophyll concentrations between January and May increase due to the weakening of iron limitation in the Southern Ocean (Figure 10b). This finding is supported by the experimentally quantified large iron release by krill (Tovar-Sanchez et al., 2007) and observations of a rapid recycling of particulate iron by copepods (Laglera et al., 2017). In our model, we only consider iron as a limiting micronutrient and the direct iron excretion or leaching fluxes from fecal pellets are converted from nitrogen excretion with a fixed Fe:N ratio. However, a recent study by Richon and Tagliabue (2021) showed that micronutrient recycling does not occur in fixed stoichiometric ratios and is further affected by food quality and food quantity. Given its role in sustaining primary production (Figure 5), a more detailed parametrization of zooplankton micronutrient recycling as in Richon and Tagliabue (2021) would be well justified.

4.2. The Role of Zooplankton Processes in Bloom Phenology

The Critical Depth Hypothesis proposes that spring phytoplankton blooms are initiated as a consequence of MLD shoaling and thus triggered by an increase in light availability (Sverdrup, 1953). However, Behrenfeld (2010) argued that this theory is not sufficient to explain phytoplankton seasonal dynamics. Specifically, the authors proposed in their "Dilution–Recoupling Hypothesis" that a bloom is initiated when growth rates are larger than loss rates and that a dilution of grazers during maximum winter MLD reduces grazing pressure to an extent that triggers the start of the spring bloom. Our two numerical experiments are a good example of the importance of the ecosystem structure on phytoplankton bloom dynamics. In the set-up with only one zooplankton group, the start of the spring bloom in the Southern Ocean depends on the increased light availability associated with the shoaling of the MLD (Sverdrup's "Critical Depth Hypothesis," Figure 10). In contrast, in the three zooplankton set-up, the spring bloom is initialized when the MLD is at its maximum (Behrenfeld's "Dilution–Recoupling Hypothesis").

The carbon accumulation rate-based analysis illustrates that nutrient recycling by zooplankton is an important driver for phytoplankton growth rate in the Southern Ocean (Figure 10b). The growth rate of phytoplankton is higher throughout the year in REcoM-3ZOO compared to REcoM-2 due to the weakening of iron limitation (Figures 10g and 10h). While summer chlorophyll concentrations increase for both phytoplankton groups due to alleviated iron limitation, winter chlorophyll concentrations decrease due to the enhanced grazing pressure. The magnitude of the spring peak in productivity increases for small phytoplankton and decreases for diatoms due to the higher grazing pressure. These results are in agreement with the key role of zooplankton grazing for determining Southern Ocean phytoplankton biomass (Le Quéré et al., 2016) and phytoplankton composition (Smetacek et al., 2004).

Plankton functional type models generally estimate that the bloom peak occurs earlier than in satellite-based estimates in the Southern Ocean (Hashioka et al., 2013; Nissen & Vogt, 2021). In this context, our model results and comparison with satellite data (Figure 11) indicate that early spring blooms could be linked to the weak zooplankton grazing in biogeochemical models. Higher winter grazing rates by zooplankton (Figure 10f) delay the BSD

by 21 days in our model (Figure 11). Our analysis illustrates that the choice of method on phytoplankton bloom phenology indicators can lead to different conclusions. While the chlorophyll-based threshold method (Siegel et al., 2002) indicates a delay of the bloom start due to grazing, the carbon accumulation rate based analysis (Llort et al., 2015) suggests that the bloom onset is unchanged, but grazing prolongs the duration between climax and apex (Figure 10b). Both methods, however, agree on a prolongation of the bloom by zooplankton grazing. Our findings support the previous conclusions by Prowe et al. (2012) and Sailley et al. (2013) that marine ecosystem models are highly sensitive to zooplankton parametrization.

The spring bloom terminates due to exhaustion of surface nutrients or overgrazing by heterotrophs (Banse, 1992, 2002). In the one-zooplankton set-up, we can observe the exhaustion of surface nutrients in early summer, since there is low grazing pressure on phytoplankton. This causes a bloom termination at the beginning of January. When we have three zooplankton types in the system, bloom termination occurs later. Fast nutrient recycling in the system increases summer chlorophyll concentrations, and at the same time zooplankton grazing prevents overuse of the nutrients by phytoplankton. Therefore, chlorophyll concentrations stay close to the threshold value (Figure 11) until the end of May, which is a further indicator of a longer bloom duration.

4.3. Implications for Biogeochemical Modeling

Representation of zooplankton is one of the grand challenges of biogeochemical modeling. This is because the performance of the zooplankton compartment in models is difficult to assess against field observations since the temporal and spatial resolution of the observations does not resemble the models (Everett et al., 2017). Furthermore, its computational cost, uncertainties in parameter estimations, and difficulties of representation of subscale processes such as swarming and vertical migration cause underrepresentation of the zooplankton in the model (Anderson, 2005). As a result, the representation of zooplankton groups varies broadly among the models. In the most simplistic models, zooplankton processes are represented implicitly (Dunne et al., 2013), or with only one explicit group (Ilyina et al., 2013). Recently, some models use two or more zooplankton functional groups to represent processes such as grazing, sinking particle formation and nutrient recycling better (Aumont et al., 2015; Le Quéré et al., 2016; Stock et al., 2020; Yool et al., 2013). It is undisputed that realistic parameter choice is the foundation of setting up a useful plankton functional type model (Anderson, 2005). However, experimental results and field studies as well as the assumptions needed to derive parameter values from these studies have significant uncertainties (Kremer et al., 2017). Modelers may choose to tune their models within these uncertainty ranges. Besides, an unresolved open question in the ocean biogeochemical modeling community is how much complexity should be represented in a model and whether the added value justifies the additional computational costs (Anderson, 2005; Friedrichs et al., 2007; Kriest et al., 2010; Kwiatkowski et al., 2014; Le Quéré, 2006). On the one hand, a comparison of 12 models with different numbers of PFTs showed that models with more multiple plankton functional types are more suitable for simulating ecosystems in different environments ("portability") than simpler models (Friedrichs et al., 2007). On the other hand, results from Kwiatkowski et al. (2014) and Kriest et al. (2010) suggest that lower biological complexity implies less biases in comparison to global nutrient or oxygen data sets. However, Xiao and Friedrichs (2014) found that simple models with only a single zooplankton size class may reproduce observed data fields by using unrealistic parameters. In agreement with these authors, we show that our implementation of multiple zooplankton functional groups provides the needed flexibility to choose parameters realistically and leads to reduced model-data mismatch with respect to global patterns of nutrients and chlorophyll, (i.e., similar metrics as used in Kwiatkowski et al. (2014) and Kriest et al. (2010)). With the advent of the MAREDAT data compilations (Buitenhuis et al., 2010; Moriarty & O'Brien, 2013; Moriarty et al., 2013), three zooplankton groups can now be reasonably simulated. In addition, we demonstrate that metrics that go beyond global nutrient and chlorophyll patterns, such as regional phytoplankton phenology can add additional insights and provide support for a representation of multiple zPFTs. Correctly representing these processes is important for robust projections of how marine ecosystem changes respond to environmental change. However, we note that it remains difficult to reproduce observed biomass, grazing fraction of NPP and use realistic parameters for all zPFTs simultaneously (Section 3.3). For the next step-change in plankton functional type modeling, robust observation-based constraints on process rates are needed. This holds true for the zooplankton processes that are traditionally considered (nutrient excretion, sloppy feeding, fecal pellet production, etc.), but also extends beyond these, for example, for diel vertical migration, food quality and life cycle (Steinberg & Landry, 2017).

Our results confirm that model results are sensitive to the zooplankton parameterization as shown previously (Laufkötter et al., 2016; Mitra et al., 2014; Prowe et al., 2012). Going beyond these previous studies, we show that high zooplankton biomass can lead to either an increase in phytoplankton concentration due to nutrient recycling or a decrease due to high grazing pressure. In addition, the increase of zooplankton biomass does not directly translate into more grazing loss of phytoplankton in the model (e.g., between 20°N and 20°S, Figures 6 and 7). Temperature dependencies of grazing parameters of zooplankton play an important role in determining the grazing loss of phytoplankton (Figure 9). This result clearly emphasizes the importance of using robust data-driven process formulations and temperature dependencies to capture the delicate balance between zooplankton processes that enhance or reduce phytoplankton growth and biomass in models. Therefore, it will be important to get more observations for evaluating the underlying processes.

Implementing multiple zPFTs in biogeochemical models provides the flexibility to assign different parameter values for different zooplankton groups (Séférian et al., 2020). When the zooplankton compartment is represented by only one group, grazing and nutrient recycling by zooplankton are not adequately represented on the global scale (Figure 7). When parameterizing multiple zPFTs, these processes are better captured, with more realistic ecosystem interactions. We demonstrated that increasing the complexity and zooplankton process representation in FESOM-RecoM not only increases understanding of the interactions of the ecosystem, but also practically provides better agreement with observations. This can be a gradual change such as a decrease of the positive bias in DIN concentration in the subtropical Pacific and a reduction of the surface chlorophyll concentration bias in the Arctic (Figure 5), but also a substantial change and a better agreement with observations as seen in the seasonal cycle of phytoplankton chlorophyll in the Southern Ocean (Figure 11).

While models capture the mean surface chlorophyll concentrations within reasonable bounds, the processes behind similar results can be very different. Our case study on the Southern Ocean phytoplankton bloom phenology also illustrates such a case. The annual mean surface chlorophyll concentrations are similar in two different simulations except for the Arctic (Figure 5). However, the seasonal cycle of chlorophyll concentrations differs between the two simulations (Figure 11). Our results emphasize that phytoplankton bloom phenology is sensitive to the representation of zooplankton grazing and nutrient recycling.

Zooplankton is generally treated as a top closure term in ocean biogeochemical models (Edwards & Yool, 2000), which causes underestimation of predation of potential competitors among zooplankton (Mitra, 2009). In REcoM-3ZOO, this ecological interaction is represented to some extent with predation of meso- and macrozooplankton on microzooplankton. However, the mortality terms for macrozooplankton (and mesozooplankton in temperate regions) are still the top closure terms. REcoM-2 and REcoM-3ZOO do not account for the interaction between zooplankton and larger predators such as fish, birds and mammals. In both model versions, we mimic the predation by higher trophic levels with the mortality term of the zooplankton groups, which remains an unavoidable simplification.

5. Conclusion

In conclusion, representing new zPFTs in an ocean biogeochemical model has a strong impact on the seasonal dynamics of phytoplankton, food web structure, and elemental cycles. Our results highlight the importance of zooplankton micronutrient recycling for global primary production and bloom duration and end date in the Southern Ocean. In addition, zooplankton grazing controls the BSD, thus supporting the Dilution-Recoupling hypothesis (Behrenfeld, 2010) and the magnitude of the spring peak. To represent the main functions of nutrient recycling, grazing, and sinking particulate organic carbon production (fecal pellets) by zooplankton in the global ocean, it is essential that biogeochemical models represent more than one zooplankton group.

Data Availability Statement

MAREDAT products are available at https://doi.org/10.1594/PANGAEA.779970, https://doi.org/10.1594/PANGAEA.785501, and https://doi.org/10.1594/PANGAEA.777398. WOA18 products are available at https://www.nodc.noaa.gov/OC5/woa18/woa18data.html. Chlorophyll data is available at https://www.oceancolour.org/ and net primary production data is available at http://sites.science.oregonstate.edu/ocean.productivity/index.php. The authors acknowledge open access to the data sets. The model results that are used in this study can be downloaded from https://doi.pangaea.de/10.1594/PANGAEA.942192.

Acknowledgments
This research was supported under the Initiative and Networking Fund of the Helmholtz Association (Helmholtz Young Investigator Group Marine Carbon and Ecosystem Feedbacks in the Earth System [MarESys], Grant VH-NG-1301). Open Access funding enabled and organized by Projekt DEAL.

References

Alcaraz, M., Almeda, R., Calbet, A., Saiz, E., Duarte, C. M., Lasternas, S., et al. (2010). The role of Arctic zooplankton in biogeochemical cycles: Respiration and excretion of ammonia and phosphate during summer. *Polar Biology*, *33*(12), 1719–1731. https://doi.org/10.1007/s00300-010-0789-9

Anderson, T. R. (2005). Plankton functional type modelling: Running before we can walk? *Journal of Plankton Research*, *27*(11), 1073–1081. https://doi.org/10.1093/plankt/fbi076

Anderson, T. R., Hessen, D. O., Mitra, A., Mayor, D. J., & Yool, A. (2013). Sensitivity of secondary production and export flux to choice of trophic transfer formulation in marine ecosystem models. *Journal of Marine Systems*, *125*, 41–53. https://doi.org/10.1016/j.jmarsys.2012.09.008

Archibald, K. M., Siegel, D. A., & Doney, S. C. (2019). Modeling the impact of zooplankton diel vertical migration on the carbon export flux of the biological pump. *Global Biogeochemical Cycles*, *33*(2), 181–199. https://doi.org/10.1029/2018GB005983

Atkinson, A., Meyer, B., Stuübing, D., Hagen, W., Schmidt, K., & Bathmann, U. V. (2002). Feeding and energy budgets of Antarctic krill *Euphausia superba* at the onset of winter-II. Juveniles and adults. *Limnology & Oceanography*, *47*(4), 953–966. https://doi.org/10.4319/lo.2002.47.4.0953

Aumont, O., Ethé, C., Tagliabue, A., Bopp, L., & Gehlen, M. (2015). PISCES-v2: An ocean biogeochemical model for carbon and ecosystem studies. *Geoscientific Model Development*, *8*(8), 2465–2513. https://doi.org/10.5194/gmd-8-2465-2015

Banse, K. (1992). Grazing, temporal changes of phytoplankton concentrations, and the microbial loop in the open sea. In P. G. Falkowski, A. D. Woodhead, & K. Vivirito (Eds.), *Primary productivity and biogeochemical cycles in the sea*. Springer. https://doi.org/10.1007/978-1-4899-0762-2_22

Banse, K. (1994). Grazing and zooplankton production as key controls of phytoplankton production in the open ocean. *Oceanography*, *7*(1), 13–20. https://doi.org/10.5670/oceanog.1994.10

Banse, K. (2002). Steemann Nielsen and the zooplankton. *Hydrobiologia*, *480*(1/3), 15–28. https://doi.org/10.1023/A:1021220714899

Banse, K. (2013). Reflections about chance in my career, and on the top-down regulated world. *Annual Review of Marine Science*, *5*, 1–19. https://doi.org/10.1146/annurev-marine-121211-172359

Behrenfeld, M. J. (2010). Abandoning Sverdrup's critical depth hypothesis on phytoplankton blooms. *Ecology*, *91*(4), 977–989. https://doi.org/10.1890/09-1207.1

Behrenfeld, M. J., & Boss, E. S. (2018). Student's tutorial on bloom hypotheses in the context of phytoplankton annual cycles. *Global Change Biology*, *24*(1), 55–77. https://doi.org/10.1111/gcb.13858

Behrenfeld, M. J., Doney, S. C., Lima, I., Boss, E. S., & Siegel, D. A. (2013). Annual cycles of ecological disturbance and recovery underlying the subarctic Atlantic spring plankton bloom. *Global Biogeochemical Cycles*, *27*(2), 526–540. https://doi.org/10.1002/gbc.20050

Behrenfeld, M. J., & Falkowski, P. G. (1997). Photosynthetic rates derived from satellite-based chlorophyll concentration. *Limnology & Oceanography*, *42*(1), 1–20. https://doi.org/10.4319/lo.1997.42.1.0001

Böckmann, S., Koch, F., Meyer, B., Pausch, F., Iversen, M., Driscoll, R., et al. (2021). Salp fecal pellets release more bioavailable iron to Southern Ocean phytoplankton than krill fecal pellets. *Current Biology*, *31*(13), 2737–2746. https://doi.org/10.1016/j.cub.2021.02.033

Buitenhuis, E., Hashioka, T., & Quéré, C. L. (2013). Combined constraints on global ocean primary production using observations and models. *Global Biogeochemical Cycles*, *27*(3), 847–858. https://doi.org/10.1002/gbc.20074

Buitenhuis, E., Le Quéré, C., Aumont, O., Beaugrand, G., Bunker, A., Hirst, A., et al. (2006). Biogeochemical fluxes through mesozooplankton. *Global Biogeochemical Cycles*, *20*(2). https://doi.org/10.1029/2005GB002511

Buitenhuis, E., Rivkin, R. B., Séailley, S., & Le Quéré, C. (2010). Biogeochemical fluxes through microzooplankton. *Global Biogeochemical Cycles*, *24*(4). https://doi.org/10.1029/2009GB003601

Calbet, A. (2001). Mesozooplankton grazing effect on primary production: A global comparative analysis in marine ecosystems. *Limnology & Oceanography*, *46*(7), 1824–1830. https://doi.org/10.4319/lo.2001.46.7.1824

Calbet, A. (2008). The trophic roles of microzooplankton in marine systems. *ICES Journal of Marine Science*, *65*(3), 325–331. https://doi.org/10.1093/icesjms/fsn013

Calbet, A., & Landry, M. R. (1999). Mesozooplankton influences on the microbial food web: Direct and indirect trophic interactions in the oligo-trophic open ocean. *Limnology & Oceanography*, *44*(6), 1370–1380. https://doi.org/10.4319/lo.1999.44.6.1370

Calbet, A., & Landry, M. R. (2004). Phytoplankton growth, microzooplankton grazing, and carbon cycling in marine systems. *Limnology & Oceanography*, *49*(1), 51–57. https://doi.org/10.4319/lo.2004.49.1.0051

Carlson, C. A., & Hansell, D. A. (2015). Chapter 3 - DOM sources, sinks, reactivity, and budgets. In D. A. Hansell & C. A. Carlson (Eds.), *Biogeochemistry of marine dissolved organic matter* (Second Edition, pp. 65–126). Academic Press. https://doi.org/10.1016/B978-0-12-405940-5.00003-0

Carr, M.-E., Friedrichs, M. A., Schmeltz, M., Noguchi Aita, M., Antoine, D., Arrigo, K. R., et al. (2006). A comparison of global estimates of marine primary production from ocean color. *Deep-Sea Research Part II: Topical Studies in Oceanography*, *53*(5), 741–770. https://doi.org/10.1016/j.dsr2.2006.01.028

Cavan, E. L., Belcher, A., Atkinson, A., Hill, S. L., Kawaguchi, S., McCormack, S., et al. (2019). The importance of Antarctic krill in biogeochemical cycles. *Nature Communications*, *10*(1), 1–13. https://doi.org/10.1038/s41467-019-12668-7

Chenillat, F., Rivière, P., & Ohman, M. D. (2021). On the sensitivity of plankton ecosystem models to the formulation of zooplankton grazing. *PLoS One*, *16*(5), e0252033. https://doi.org/10.1371/journal.pone.0252033

Coello-Camba, A., Llabrés, M., Duarte, C. M., & Agustí, S. (2017). Zooplankton excretion metabolites stimulate Southern Ocean phytoplankton growth. *Polar Biology*, *40*(10), 2035–2045. https://doi.org/10.1007/s00300-017-2123-2

Dunne, J. P., John, J. G., Shevliakova, E., Stouffer, R. J., Krasting, J. P., Malyshev, S. L., et al. (2013). GFDL's ESM2 global coupled climate–carbon Earth system models. Part II: Carbon system formulation and baseline simulation characteristics. *Journal of Climate*, *26*(7), 2247–2267. https://doi.org/10.1175/JCLI-D-12-00150.1

Dunne, J. P., Sarmiento, J. L., & Gnanadesikan, A. (2007). A synthesis of global particle export from the surface ocean and cycling through the ocean interior and on the seafloor. *Global Biogeochemical Cycles*, *21*(4). https://doi.org/10.1029/2006GB002907

Edwards, A. M., & Yool, A. (2000). The role of higher predation in plankton population models. *Journal of Plankton Research*, *22*(6), 1085–1112. https://doi.org/10.1093/plankt/22.6.1085

Everett, J. D., Baird, M. E., Buchanan, P., Bulman, C., Davies, C., Downie, R., et al. (2017). Modeling what we sample and sampling what we model: Challenges for zooplankton model assessment. *Frontiers in Marine Science*, *4*, 77. https://doi.org/10.3389/fmars.2017.00077

Friedrichs, M. A. M., Dusenberry, J. A., Anderson, L. A., Armstrong, R. A., Chai, F., Christian, J. R., et al. (2007). Assessment of skill and portability in regional marine biogeochemical models: Role of multiple planktonic groups. *Journal of Geophysical Research*, *112*(C8), C08001. https://doi.org/10.1029/2006JC003852

Froneman, P., & Perissinotto, R. (1996). Microzooplankton grazing in the Southern Ocean: Implications for the carbon cycle. *Marine Ecology*, *17*(1–3), 99–115. https://doi.org/10.1111/j.1439-0485.1996.tb00493.x

Frost, B. W. (1987). Grazing control of phytoplankton stock in the open subarctic Pacific ocean: A model assessing the role of mesozooplankton, particularly the large calanoid copepods *Neocalanus spp*. *Marine Ecology Progress Series*, *39*(1), 49–68. https://doi.org/10.3354/meps039049

Frost, B. W. (1991). The role of grazing in nutrient-rich areas of the open sea. *Limnology & Oceanography*, *36*(8), 1616–1630. https://doi.org/10.4319/lo.1991.36.8.1616

Frost, B. W. (1993). A modelling study of processes regulating plankton standing stock and production in the open subarctic Pacific Ocean. *Progress in Oceanography*, *32*(1–4), 17–56. https://doi.org/10.1016/0079-6611(93)90008-2

Garcia, H. E., Weathers, K. W., Paver, C. R., Smolyar, I., Boyer, T. P., Locarnini, R., et al. (2018). World Ocean Atlas 2018. Volume 4: Dissolved inorganic nutrients (phosphate, nitrate and nitrate+nitrite, silicate). *NOAA Atlas NESDIS*, *84*, 35.

Garcia, Locarnini, R., Boyer, T. P., Antonov, J. I., Baranova, O. K., Zweng, M. M., et al. (2013). World Ocean Atlas 2013 volume 4: Nutrients (phosphate, nitrate, silicate). *NOAA Atlas NESDIS*, *76*, 396.

Geider, R. J., Maclntyre, H. L., & Kana, T. M. (1998). A dynamic regulatory model of phytoplanktonic acclimation to light, nutrients, and temperature. *Limnology & Oceanography*, *43*(4), 679–694. https://doi.org/10.4319/lo.1998.43.4.0679

Gowing, M. M., & Silver, M. W. (1985). Minipellets: A new and abundant size class of marine fecal pellets. *Journal of Marine Research*, *43*(2), 395–418. https://doi.org/10.1357/002224085788438676

Griffies, S. M., Biastoch, A., Böning, C., Bryan, F., Danabasoglu, G., Chassignet, E. P., et al. (2009). Coordinated ocean-ice reference experiments (COREs). *Ocean Modelling*, *26*(1), 1–46. https://doi.org/10.1016/j.ocemod.2008.08.007

Hansen, B., Bjornsen, P. K., & Hansen, P. J. (1994). The size ratio between planktonic predators and their prey. *Limnology & Oceanography*, *39*(2), 395–403. https://doi.org/10.4319/lo.1994.39.2.0395

Hashioka, T., Vogt, M., Yamanaka, Y., Le Quéré, C., Buitenhuis, E. T., Aita, M. N., et al. (2013). Phytoplankton competition during the spring bloom in four plankton functional type models. *Biogeosciences*, *10*(11), 6833–6850. https://doi.org/10.5194/bg-10-6833-2013

Hauck, J., Völker, C., Wang, T., Hoppema, M., Losch, M., & Wolf-Gladrow, D. A. (2013). Seasonally different carbon flux changes in the Southern Ocean in response to the southern annular mode. *Global Biogeochemical Cycles*, *27*(4), 1236–1245. https://doi.org/10.1002/2013GB004600

Henson, S. A., Dunne, J. P., & Sarmiento, J. L. (2009). Decadal variability in north Atlantic phytoplankton blooms. *Journal of Geophysical Research*, *114*(C4), C04013. https://doi.org/10.1029/2008JC005139

Henson, S. A., Sanders, R., Madsen, E., Morris, P. J., Le Moigne, F., & Quartly, G. D. (2011). A reduced estimate of the strength of the ocean's biological carbon pump. *Geophysical Research Letters*, *38*(4). https://doi.org/10.1029/2011GL046735

Hernández-León, S., Fraga, C., & Ikeda, T. (2008). A global estimation of mesozooplankton ammonium excretion in the open ocean. *Journal of Plankton Research*, *30*(5), 577–585. https://doi.org/10.1093/plankt/fbn021

Hofmann, E. E., & Lascara, C. M. (2000). Modeling the growth dynamics of Antarctic krill *Euphausia superba*. *Marine Ecology Progress Series*, *194*, 219–231. https://doi.org/10.3354/meps194219

Ikeda, T. (2014). Respiration and ammonia excretion by marine metazooplankton taxa: Synthesis toward a global-bathymetric model. *Marine Biology*, *161*(12), 2753–2766. https://doi.org/10.1007/s00227-014-2540-5

Ilyina, T., Six, K. D., Segschneider, J., Maier-Reimer, E., Li, H., & Núñez-Riboni, I. (2013). Global ocean biogeochemistry model HAMOCC: Model architecture and performance as component of the MPI-Earth system model in different CMIP5 experimental realizations. *Journal of Advances in Modeling Earth Systems*, *5*(2), 287–315. https://doi.org/10.1029/2012MS000178

Johnson, R., Strutton, P. G., Wright, S. W., McMinn, A., & Meiners, K. M. (2013). Three improved satellite chlorophyll algorithms for the Southern Ocean. *Journal of Geophysical Research: Oceans*, *118*(7), 3694–3703. https://doi.org/10.1002/jgrc.20270

Karakuş, O., Völker, C., Iversen, M., Hagen, W., Wolf-Gladrow, D., Fach, B., & Hauck, J. (2021). Modeling the impact of macrozooplankton on carbon export production in the Southern Ocean. *Journal of Geophysical Research: Oceans*, *126*(12). https://doi.org/10.1029/2021JC017315

Kiørboe, T. (1997). Population regulation and role of mesozooplankton in shaping marine pelagic food webs. *Hydrobiologia*, *363*(1/3), 13–27. https://doi.org/10.1023/A:1003173721751

Kiørboe, T., Møhlenberg, F., & Hamburger, K. (1985). Bioenergetics of the planktonic copepod *Acartia tonsa*: Relation between feeding, egg production and respiration, and the composition of specific dynamic action. *Marine Ecology Progress Series*, *26*(1–2), 85–97. https://doi.org/10.3354/meps026085

Kobayashi, S., Ota, Y., Harada, Y., Ebita, A., Moriya, M., Onoda, H., et al. (2015). The JRA-55 reanalysis: General specifications and basic characteristics. *Journal of the Meteorological Society of Japan*, *93*(1), 5–48. https://doi.org/10.2151/jmsj.2015-001

Kremer, C. T., Thomas, M. K., & Litchman, E. (2017). Temperature- and size-scaling of phytoplankton population growth rates: Reconciling the Eppley curve and the metabolic theory of ecology. *Limnology & Oceanography*, *62*(4), 1658–1670. https://doi.org/10.1002/lno.10523

Kriest, I., Khatiwala, S., & Oschlies, A. (2010). Towards an assessment of simple global marine biogeochemical models of different complexity. *Progress in Oceanography*, *86*(3), 337–360. https://doi.org/10.1016/j.pocean.2010.05.002

Kulk, G., Platt, T., Dingle, J., Jackson, T., Jönsson, B. F., Bouman, H. A., et al. (2021). Correction: Kulk et al. Primary Production, an Index of Climate Change in the Ocean: Satellite-Based Estimates over Two Decades. Remote Sens. 2020, 12, 826. *Remote Sensing*, *13*(17), 3462. https://doi.org/10.3390/rs13173462

Kwiatkowski, L., Yool, A., Allen, J. I., Anderson, T. R., Barciela, R., Buitenhuis, E. T., et al. (2014). IMarNet: An ocean biogeochemistry model intercomparison project within a common physical ocean modelling framework. *Biogeosciences*, *11*(24), 7291–7304. https://doi.org/10.5194/bg-11-7291-2014

Laglera, L. M., Tovar-Sánchez, A., Iversen, M., González, H., Naik, H., Mangesh, G., et al. (2017). Iron partitioning during LOHAFEX: Copepod grazing as a major driver for iron recycling in the Southern Ocean. *Marine Chemistry*, *196*, 148–161. https://doi.org/10.1016/j.marchem.2017.08.011

Landry, M. R., & Calbet, A. (2004). Microzooplankton production in the oceans. *ICES Journal of Marine Science*, *61*(4), 501–507. https://doi.org/10.1016/j.icesjms.2004.03.011

Laufkötter, C., Vogt, M., Gruber, N., Aumont, O., Bopp, L., Doney, S. C., et al. (2016). Projected decreases in future marine export production: The role of the carbon flux through the upper ocean ecosystem. *Biogeosciences*, *13*(13), 4023–4047. https://doi.org/10.5194/bg-13-4023-2016

Lauvset, S. K., Key, R. M., Olsen, A., Van Heuven, S., Velo, A., Lin, X., et al. (2016). A new global interior ocean mapped climatology: The 1° x 1° GLODAP version 2. *Earth System Science Data*, *8*(2), 325–340. https://doi.org/10.5194/essd-8-325-2016

Leblanc, K., Arístegui, J., Armand, L., Assmy, P., Beker, B., Bode, A., et al. (2012). A global diatom database – Abundance, biovolume and biomass in the world ocean. *Earth System Science Data*, *4*(1), 149–165. https://doi.org/10.5194/essd-4-149-2012

Lee, K. (2001). Global net community production estimated from the annual cycle of surface water total dissolved inorganic carbon. *Limnology & Oceanography*, *46*(6), 1287–1297. https://doi.org/10.4319/lo.2001.46.6.1287

Le Quéré, C. (2006). Reply to horizons article 'plankton functional type modelling: Running before we can walk' Anderson (2005): I. Abrupt changes in marine ecosystems? *Journal of Plankton Research*, *28*(9), 871–872. https://doi.org/10.1093/plankt/fbl014

Le Quéré, C., Buitenhuis, E. T., Moriarty, R., Alvain, S., Aumont, O., Bopp, L., et al. (2016). Role of zooplankton dynamics for Southern Ocean phytoplankton biomass and global biogeochemical cycles. *Biogeosciences*, *13*(14), 4111–4133. https://doi.org/10.5194/bg-13-4111-2016

Le Quéré, C., Harrison, S. P., Colin Prentice, I., Buitenhuis, E. T., Aumont, O., Bopp, L., et al. (2005). Ecosystem dynamics based on plankton functional types for global ocean biogeochemistry models. *Global Change Biology*, *11*(11), 2016–2040. https://doi.org/10.1111/j.1365-2486.2005.1004.x

Llort, J., Lévy, M., Sallée, J.-B., & Tagliabue, A. (2015). Onset, intensification, and decline of phytoplankton blooms in the Southern Ocean. *ICES Journal of Marine Science*, *72*(6), 1971–1984. https://doi.org/10.1093/icesjms/fsv053

Menden-Deuer, S., Slade, W. H., & Dierssen, H. (2021). Promoting instrument development for new research avenues in ocean science: Opening the black box of grazing. *Frontiers in Marine Science*, *8*. https://doi.org/10.3389/fmars.2021.695938

Mitra, A. (2009). Are closure terms appropriate or necessary descriptors of zooplankton loss in nutrient-phytoplankton-zooplankton type models? *Ecological Modelling*, *220*(5), 611–620. https://doi.org/10.1016/j.ecolmodel.2008.12.008

Mitra, A., Castellani, C., Gentleman, W. C., Jónasdóttir, S. H., Flynn, K. J., Bode, A., et al. (2014). Bridging the gap between marine biogeochemical and fisheries sciences; configuring the zooplankton link. *Progress in Oceanography*, *129*(PB), 176–199. https://doi.org/10.1016/j.pocean.2014.04.025

Møller, E. F. (2007). Production of dissolved organic carbon by sloppy feeding in the copepods *Acartia tonsa*, *Centropages typicus*, and *Temora longicornis*. *Limnology & Oceanography*, *52*(1), 79–84. https://doi.org/10.4319/lo.2007.52.1.0079

Montagnes, D. J., & Fenton, A. (2012). Prey-abundance affects zooplankton assimilation efficiency and the outcome of biogeochemical models. *Ecological Modelling*, *243*, 1–7. https://doi.org/10.1016/j.ecolmodel.2012.05.006

Morales, C. (1987). Carbon and nitrogen content of copepod faecal pellets: Effect of food concentration and feeding behavior. *Marine Ecology Progress Series*, *36*, 107–114. https://doi.org/10.3354/meps036107

Moriarty, R., Buitenhuis, E. T., Le Quéré, C., & Gosselin, M. P. (2013). Distribution of known macrozooplankton abundance and biomass in the global ocean. *Earth System Science Data*, *5*(2), 241–257. https://doi.org/10.5194/essd-5-241-2013

Moriarty, R., & O'Brien, T. D. (2013). Distribution of mesozooplankton biomass in the global ocean. *Earth System Science Data*, *5*(1), 45–55. https://doi.org/10.5194/essd-5-45-2013

Mullin, M. M. (1963). Some factors affecting the feeding of marine copepods of the *genus Calanus*. *Limnology & Oceanography*, *8*(2), 239–250. https://doi.org/10.4319/lo.1963.8.2.0239

Nissen, C., & Vogt, M. (2021). Factors controlling the competition between *Phaeocystis* and diatoms in the Southern Ocean and implications for carbon export fluxes. *Biogeosciences*, *18*(1), 251–283. https://doi.org/10.5194/bg-18-251-2021

Prowe, A., Pahlow, M., Dutkiewicz, S., Follows, M., & Oschlies, A. (2012). Top-down control of marine phytoplankton diversity in a global ecosystem model. *Progress in Oceanography*, *101*(1), 1–13. https://doi.org/10.1016/j.pocean.2011.11.016

Racault, M.-F., Le Quéré, C., Buitenhuis, E., Sathyendranath, S., & Platt, T. (2012). Phytoplankton phenology in the global ocean. *Ecological Indicators*, *14*(1), 152–163. https://doi.org/10.1016/j.ecolind.2011.07.010

Richon, C., & Tagliabue, A. (2021). Biogeochemical feedbacks associated with the response of micronutrient recycling by zooplankton to climate change. *Global Change Biology*, *27*(19), 4758–4770. https://doi.org/10.1111/gcb.15789

Roy, S., Harris, R. P., & Poulet, S. A. (1989). Inefficient feeding by *Calanus helgolandicus* and *Temora longicornis* on *Coscinodiscus wailesii*: Quantitative estimation using chlorophyll-type pigments and effects on dissolved free amino acids. *Marine Ecology Progress Series*, *52*, 145–153. https://doi.org/10.3354/meps052145

Saba, G. K., Steinberg, D. K., & Bronk, D. A. (2009). Effects of diet on release of dissolved organic and inorganic nutrients by the copepod *Acartia tonsa*. *Marine Ecology Progress Series*, *386*, 147–161. https://doi.org/10.3354/meps08070

Sailley, S., Vogt, M., Doney, S., Aita, M., Bopp, L., Buitenhuis, E., et al. (2013). Comparing food web structures and dynamics across a suite of global marine ecosystem models. *Ecological Modelling*, *261–262*, 43–57. https://doi.org/10.1016/j.ecolmodel.2013.04.006

Sathyendranath, S., Brewin, R. J., Brockmann, C., Brotas, V., Calton, B., Chuprin, A., et al. (2019). An ocean-colour time series for use in climate studies: The experience of the ocean-colour climate change initiative (OC-CCI). *Sensors*, *19*(19), 4285. https://doi.org/10.3390/s19194285

Schlitzer, R. (2004). Export production in the equatorial and north Pacific derived from dissolved oxygen, nutrient and carbon data. *Journal of Oceanography*, *60*(1), 53–62. https://doi.org/10.1023/B:JOCE.0000038318.38916.e6

Schmidt, K., Atkinson, A., Pond, D. W., & Irel, L. C. (2014). Feeding and overwintering of Antarctic Krill across its major habitats: The role of sea ice cover, water depth, and phytoplankton abundance. *Limnology & Oceanography*, *59*(1), 17–36. https://doi.org/10.4319/lo.2014.59.1.0017

Schourup-Kristensen, V., Sidorenko, D., Wolf-Gladrow, D. A., & Völker, C. (2014). A skill assessment of the biogeochemical model REcoM2 coupled to the finite Element Sea ice–Ocean Model (FESOM 1.3). *Geoscientific Model Development*, *7*(6), 2769–2802. https://doi.org/10.5194/gmd-7-2769-2014

Séférian, R., Berthet, S., Yool, A., Palmiéri, J., Bopp, L., Tagliabue, A., et al. (2020). Tracking improvement in simulated marine biogeochemistry between CMIP5 and CMIP6. *Current Climate Change Reports*, *6*(3), 95–119. https://doi.org/10.1007/s40641-020-00160-0

Sidorenko, D., Wang, Q., Danilov, S., & Schröter, J. (2011). FESOM under coordinated ocean-ice reference experiment forcing. *Ocean Dynamics*, *61*(7), 881–890. https://doi.org/10.1007/s10236-011-0406-7

Sieburth, J. M., Smetacek, V., & Lenz, J. (1978). Pelagic ecosystem structure: Heterotrophic compartments of the plankton and their relationship to plankton size fractions. *Limnology & Oceanography*, *23*(6), 1256–1263. https://doi.org/10.4319/lo.1978.23.6.1256

Siegel, D. A., Buesseler, K. O., Doney, S. C., Sailley, S. F., Behrenfeld, M. J., & Boyd, P. W. (2014). Global assessment of ocean carbon export by combining satellite observations and food-web models. *Global Biogeochemical Cycles*, *28*(3), 181–196. https://doi.org/10.1002/2013GB004743

Siegel, D. A., Doney, S. C., & Yoder, J. A. (2002). The North Atlantic spring phytoplankton bloom and Sverdrup's critical depth hypothesis. *Science*, *296*(5568), 730–733. https://doi.org/10.1126/science.1069174

Smetacek, V. (1998). Diatoms and the silicate factor. *Nature*, *391*(6664), 224–225. https://doi.org/10.1038/34528

Smetacek, V., Assmy, P., & Henjes, J. (2004). The role of grazing in structuring Southern Ocean pelagic ecosystems and biogeochemical cycles. *Antarctic Science*, *16*(4), 541–558. https://doi.org/10.1017/S0954102004002317

Soppa, M. A., Völker, C., & Bracher, A. (2016). Diatom phenology in the Southern Ocean: Mean patterns, trends and the role of climate oscillations. *Remote Sensing*, *8*(5), 1–17. https://doi.org/10.3390/rs8050420

Steinberg, D. K., & Landry, M. R. (2017). Zooplankton and the ocean carbon cycle. *Annual Review of Marine Science*, *9*(1), 413–444. https://doi.org/10.1146/annurev-marine-010814-015924

Stock, C. A., Dunne, J. P., Fan, S., Ginoux, P., John, J., Krasting, J. P., et al. (2020). Ocean biogeochemistry in GFDL's Earth system Model 4.1 and its response to increasing atmospheric CO_2. *Journal of Advances in Modeling Earth Systems*, *12*(10). https://doi.org/10.1029/2019MS002043

Sverdrup, H. U. (1953). On conditions for the vernal blooming of phytoplankton. *ICES Journal of Marine Science*, *18*(3), 287–295. https://doi.org/10.1093/icesjms/18.3.287

Taylor, K. E. (2001). Summarizing multiple aspects of model performance in a single diagram. *Journal of Geophysical Research*, *106*(D7), 7183–7192. https://doi.org/10.1029/2000JD900719

Thor, P. (2003). Elevated respiration rates of the neritic copepod *Acartia tonsa* during recovery from starvation. *Journal of Experimental Marine Biology and Ecology*, *283*(1), 133–143. https://doi.org/10.1016/S0022-0981(02)00473-2

Tovar-Sanchez, A., Duarte, C. M., Hernández-León, S., & Sañudo-Wilhelmy, S. A. (2007). Krill as a central node for iron cycling in the Southern Ocean. *Geophysical Research Letters*, *34*(11), L11601. https://doi.org/10.1029/2006GL029096

Turner, J. T. (2002). Zooplankton fecal pellets, mrine snow and sinking phytoplankton blooms. *Aquatic Microbial Ecology*, *27*, 57–102. https://doi.org/10.3354/ame027057

Turner, J. T. (2015). Zooplankton fecal pellets, marine snow, phytodetritus and the ocean's biological pump. *Progress in Oceanography*, *130*, 205–248. https://doi.org/10.1016/j.pocean.2014.08.005

Verity, P. G. (1985). Grazing, respiration, excretion, and growth rates of tintinnids. *Limnology & Oceanography*, *30*(6), 1268–1282. https://doi.org/10.4319/lo.1985.30.6.1268

Wang, Q., Danilov, S., Sidorenko, D., Timmermann, R., Wekerle, C., Wang, X., et al. (2014). The finite Element Sea ice-Ocean Model (FESOM) v.1.4: Formulation of an ocean general circulation model. *Geoscientific Model Development*, *7*(2), 663–693. https://doi.org/10.5194/gmd-7-663-2014

Westberry, T., Behrenfeld, M. J., Siegel, D. A., & Boss, E. (2008). Carbon-based primary productivity modeling with vertically resolved photoacclimation. *Global Biogeochemical Cycles*, *22*(2). https://doi.org/10.1029/2007GB003078

Wright, R. M., Le Quéré, C., Buitenhuis, E., Pitois, S., & Gibbons, M. (2020). Unique role of jellyfish in the plankton ecosystem revealed using a global ocean biogeochemical model. *Biogeosciences Discussions*, 1–43. https://doi.org/10.5194/bg-2020-136

Xiao, Y., & Friedrichs, M. A. M. (2014). Using biogeochemical data assimilation to assess the relative skill of multiple ecosystem models in the Mid-Atlantic Bight: Effects of increasing the complexity of the planktonic food web. *Biogeosciences*, *11*(11), 3015–3030. https://doi.org/10.5194/bg-11-3015-2014

Yool, A., Popova, E. E., & Anderson, T. R. (2013). MEDUSA-2.0: An intermediate complexity biogeochemical model of the marine carbon cycle for climate change and ocean acidification studies. *Geoscientific Model Development*, *6*(5), 1767–1811. https://doi.org/10.5194/gmd-6-1767-2013